TECTONICS, VOL. 7, NO. 6, PAGES 1257-1278, DECEMBER 1988

HOW MUCH DOES SLIP ON A REACTIVATED FAULT PLANE CONSTRAIN THE STRESS TENSOR ?

Bernard Célérier[1]

Department of Earth, Atmospheric and Planetary Sciences, Massachusetts Institute of Technology, Cambridge.

Abstract. Given a fault plane and its slip vector, the stress tensor which caused the displacement is sought. Two constraints are considered: first, a geometrical constraint that the shear stress applied to the fault plane is parallel to the slip (Wallace, 1951; Bott, 1959); second, a frictional constraint that the shear to normal stress ratio equals $\tan\varphi_0$ (Coulomb, 1776). In a first step, the stress tensors that satisfy the geometrical constraint are sought. For tensors belonging to the vectorial space of solutions, shear and normal stress magnitudes become a function of the orientation of the principal stresses, $\vec{s_1}$, $\vec{s_2}$, $\vec{s_3}$, and are mapped, extending a study by McKenzie (1969). In a second step, it is investigated which of these tensors also satisfy the frictional constraint. Within this more restricted vectorial space, there is a relationship between the magnitudes, $\delta = (\sigma_1 - \sigma_2)/(\sigma_1 - \sigma_3)$ and $s = (\sigma_1 - \sigma_3)/\sigma_1$, and the orientations, $\vec{s_1}$, $\vec{s_2}$, $\vec{s_3}$, of the principal stresses. Both the range of s and the spatial distribution of $\vec{s_1}$, $\vec{s_2}$, $\vec{s_3}$ are more restricted than when the geometrical constraint alone is considered. As when the geometrical constraint is solely considered (McKenzie, 1969), the orientations of the principal stresses, $\vec{s_1}$, $\vec{s_2}$, $\vec{s_3}$, may lie significantly away from and up to right angle to the P, B, T axes. However, this can happen only in two cases: (1) either the effective stress difference s has reached a high value, which is unlikely to happen if enough preexisting fractures are available to release the stress, or (2) σ_2 becomes close to either σ_1 or σ_3 and therefore barely distinguishable from it; in that case the delocalization of the orientations of the principal stresses is best described by a tendency for $\vec{s_2}$ to exchange role with either $\vec{s_1}$ or $\vec{s_3}$. When the stress difference remains small and σ_2 reasonably away from σ_1 and σ_3, $\vec{s_1}$, $\vec{s_2}$, $\vec{s_3}$ approach positions that we define as the P_f, B, T_f axes and that are obtained from the P, B, T axes by a rotation of angle $\varphi_0/2$ around B and toward the slip vector. This explains why the P, B, T axes gives reasonable estimates of the orientations of the principal stresses (Scheidegger, 1964) despite objections (McKenzie, 1969). However, whenever the fault plane can be distinguished from the auxiliary plane, P_f, B, T_f should give a better estimate (Raleigh et al., 1972). In an area where many fault planes are available and a uniform tensor is assumed, the scatter in the plane orientations contains information about both the relative position of σ_2, represented by δ, and the relative stress difference s: the higher s or the closer δ to either 0 or 1, the more scatter. This information could then be extracted by inverse methods. Because a friction law would constrain these inverse method more tightly, it may show the necessity of nonuniform tensor to explain scattered fault plane.

INTRODUCTION

To constrain the stress tensor that caused a displacement along an observed fault plane and slip direction, i.e., to determine the orientations, $\vec{s_1}$, $\vec{s_2}$, $\vec{s_3}$, and magnitudes, σ_1, σ_2, σ_3, of its principal stresses, requires some hypothesis about the failure mechanism.

The simplest such hypothesis is that fresh failure occurred within intact isotropic rocks. Using Coulomb's [1776] failure criterion, the stress orientations [Anderson, 1951] and the relative stress difference s :

[1]Now at Institute for Geophysics, University of Texas at Austin.

Paper number 8T0056.
0278-7407/88/008T-0056$10.00

$$s = (\sigma_1 - \sigma_3) / \sigma_1 \quad (1)$$

can be inverted for.

However, in geological context a preexisting plane of weakness is likely to be present within the rocks, and sliding on that plane may occur before a state of stress high enough to cause failure is reached [Wallace, 1951; Talobre, 1957; Bott, 1959; Jaeger, 1960; Donath, 1964; Handin, 1969; McKenzie, 1969]. As a result in most geological cases, the failure model is of little use, and other constraints must be sought [McKenzie, 1969].

Such a constraint can be found in the fact that the shear stress within the fault plane must parallel the slip vector [Wallace, 1951; Bott, 1959; McKenzie, 1969]. This will be referred to as the geometrical constraint in the rest of this paper. The orientation of the shear stress depends only on four parameters [Bott, 1959]: three that define the orientations of the principal stresses and the tensor aspect ratio δ that defines the relative value of σ_2 with respect to σ_1 and σ_3:

$$\delta = (\sigma_1 - \sigma_2)/(\sigma_1 - \sigma_3) \quad (2)$$

This geometrical constraint appears weak since for stress tensors satisfying it, the maximum principal stress direction $\vec{s_1}$ can lie anywhere in the dilatational quadrant of a fault plane solution [McKenzie, 1969; Angelier and Mechler, 1977]. This problem is overcome by assuming that the same stress tensor is the cause of slip on many observed fault planes and that for each fault plane this constraint holds. Theoretically, four fault planes and their associated slips should determine the orientations of the principal stresses and δ. In practice, more fault planes are used, and a minimum misfit solution to this overdetermined system is sought [Carey and Brunier, 1974; Carey, 1976, 1979; Angelier, 1975, 1979a, b; Armijo and Cisternas, 1978; Angelier and Goguel, 1979; Ellsworth and Zhonghuai, 1980; Etchecopar et al., 1981; Armijo et al., 1982; Angelier et al., 1982; Vasseur et al., 1983; Gephart and Forsyth, 1984], and in most cases, a regional uniform stress tensor solution is found acceptable.

However, the claim that no further constraint can be used in that case [McKenzie, 1969] seems unwarranted because frictional sliding requires a friction law to be satisfied [Talobre, 1957; Jaeger, 1959]. In fact, the methods based on the sole geometrical constraint allow mechanically unacceptable solutions, such as those producing a very small shear stress that is parallel to the observed slip on a fault plane but associated with a very large normal stress on that same fault plane. The question arises then, if these unacceptable solutions were thrown out, would a uniform stress tensor still be a possible solution?

An attempt to constrain this problem further considered that at rupture the shear stress τ must have reached a threshold τ_0 [Michael, 1984]. However, this choice does not correspond to a realistic failure criterion and rather seems to be motivated by the simplification that it brings to the inversion technique by linearizing the equations. Another attempt introduced a friction law but only as an inequality that must be satisfied besides minimizing the misfit between shear stress and slip [Ellsworth, 1982; Sassi, 1985].

The work presented here follows a suggestion [W. F. Brace, personal communication, 1980] that some useful insight could be gained from applying Coulomb's [1776] law of friction to constrain this problem further. This law is simple enough and reasonably independent of rock types [Byerlee, 1978]. The consequences of this extra constraint (referred to as the frictional constraint) in the case of a single fault plane are therefore derived in what follows. In a first step the description of the stress tensors satisfying the geometrical constraint is extended from the initial work of McKenzie [1969] so as to facilitate, in subsequent steps, the recognition of those among them that also satisfy the friction law. The frictional constraint is then introduced. Finally, the general three-dimensional inverse problem with both constraints together is solved. This will show that $\vec{s_1}$ is limited to a smaller range than the whole dilatational quadrant, that s is limited to values bigger than a critical value s_c, and that not only δ but also s could be inverted for in the case of multiple planes.

SETTING THE PROBLEM

The fault plane frame of reference $E = (\vec{e_1}, \vec{e_2}, \vec{e_3})$ is defined as by McKenzie [1969] (Figure 1 and Table 1): $\vec{e_1}, \vec{e_2}, \vec{e_3}$ are unit vectors; $\vec{e_3}$ is normal to the fault plane; $\vec{e_1}$ is the slip of the lower half-space ($x_3 < 0$) relatively to the upper half-space ($x_3 > 0$); $\vec{e_2} = \vec{e_3} \times \vec{e_1}$. Within that frame, A_1, A_2, A_3 are defined so that $\vec{OA_i} = \vec{e_i}$ and the P, T, B axes are defined as in seismology [Scheidegger, 1964].

Failure or friction depends only on the effective stress tensor $\underline{\underline{T}}$, which is represented in the E frame by the matrix T^E of components t^E_{ij}. A positive sign is chosen for compressive stresses as usually done in rock mechanics. The six parameters

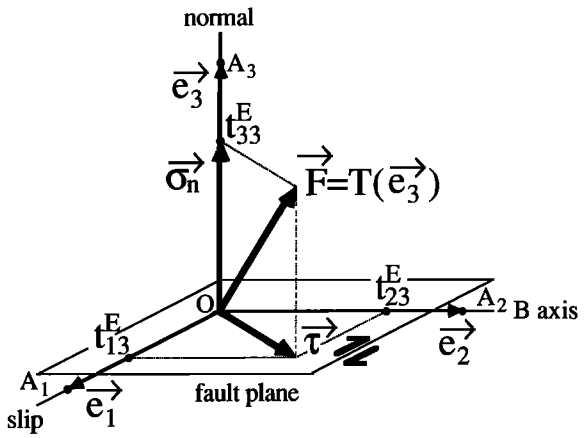

Fig. 1. The fault plane frame of reference $E = (\vec{e_1}, \vec{e_2}, \vec{e_3})$; $\vec{e_3}$ is normal to the fault plane. $\vec{e_1}$ is the slip of the lower half-space ($x_3 < 0$) relatively to the upper half-space ($x_3 > 0$). $\vec{F}$ is the stress applied to the upper half-space. Other symbols are defined in Table 1.

TABLE 1. Symbols

Symbols	Comments
	General conventions
$\underline{\underline{A}}$	operator
$\underline{\underline{A}}^B$	matrix of operator $\underline{\underline{A}}$ (or frame A) in frame B
a_{ij}^B	components of matrix A in frame B
$\vec{v}$	vector
v	magnitude of $\vec{v}$
	Fault plane frame
$E = (\vec{e_1}, \vec{e_2}, \vec{e_3})$	Slip and fault plane frame (Figure 1)
A_1, A_2, A_3	endpoints of unit vectors: $\vec{OA_i} = \vec{e_i}$ (Figure 1)
P, B, T	defined as in seismology [Scheidegger, 1964] (Figure 6b)
	Stress tensor
$\underline{\underline{T}}$	effective stress tensor
$\underline{\underline{T}}_d$	reduced stress tensor (equation (5))
$S = (\vec{s_1}, \vec{s_2}, \vec{s_3})$	principal stresses frame (eigenvectors of $\underline{\underline{T}}$)
$\sigma_1 \geq \sigma_2 \geq \sigma_3$	magnitudes of the principal effective stresses (eigenvalues of $\underline{\underline{T}}$)
$s = (\sigma_1 - \sigma_3)/\sigma_1$	relative stress difference (equation (1))
$\delta = (\sigma_1 - \sigma_2)/(\sigma_1 - \sigma_3)$	tensor aspect ratio or relative position of σ_2 (Figure 3b; equation (2))
θ_1	angular representation of δ (Figure 3; equation (8))
$\vec{F}$	stress applied to the fault plane of normal $\vec{e_3}$ (Figure 1; equation (12))
$\vec{\tau}$	shear stress on the fault plane (Figure 1; equation (14))
$\vec{\sigma_n}$	normal stress on the fault plane (Figure 1; equation (13))
	Coulomb's criterion
τ_0	cohesion (Figure 6a; equation (34))
φ_0	friction angle (Figure 6a; equation (34)); in the figures $\varphi_0 = 31°$ (equation (44))
$H = \tau - \tan\varphi_0 \bullet \sigma_n$	$H = \tau_0$ is Coulomb's criteria (equations (15) and (34))
$s' = (\sigma_1-\sigma_3)/(\sigma_1+\tau_0/\tan\varphi_0)$	modified stress difference (if $\tau_0 = 0$ then $s' = s$) for the failure criteria (equation (39))
$s_c = 2\tan\varphi_0/\tan\varphi_1$	minimum stress difference for slip; $s_c = 0.679$ (equation (52))
P_f, B, T_f	most efficient orientation of $\vec{s_1}, \vec{s_2}, \vec{s_3}$ to produces sliding (Figure 6b)
$\varphi_1 = \varphi_0/2 + \pi/4$	angle between P_f and $\vec{e_3}$ and between $-\vec{e_1}$ and T_f (Figure 6b; equation (36))
	Other variables
θ, φ, ψ	Euler's angles transforming E into S (Figure 2)
R_G	area where $\vec{s_1}$ must be to satisfy the geometrical constraint (Figure 4c)
$D(\theta_1), D''(\theta_1), D'''(\theta_1)$	$\vec{s_1}, \vec{s_2}, \vec{s_3}$ trajectories when $\psi_1(\theta,\varphi,\delta) = \psi_2(\theta,\varphi,\delta)$ (Figure 5)
$\varepsilon = \pm 1$	+1 or -1 if ψ_1 or ψ_2 (equation (25) or (26)) are respectively substituted for ψ (equation (29))
$C(\alpha)$	great circle in plane at angle α from $\vec{e_3}$ (Figure 4b)

that define the stress tensor $\underline{\underline{T}}$ can be broken into two categories: the three magnitudes of the principal stresses: σ_1, σ_2, σ_3 that are the eigenvalues of $\underline{\underline{T}}$ ordered so that $\sigma_1 \geq \sigma_2 \geq \sigma_3$; and the three parameters that define the frame $S = (\vec{s_1}, \vec{s_2}, \vec{s_3})$ that is a direct set of unit eigenvectors of $\underline{\underline{T}}$ corresponding to the respective eigenvalue $\sigma_1, \sigma_2, \sigma_3$. The orientation of that frame will be represented by an equal area azimuthal projection [Lambert, 1772] into the fault plane that is facilitated by requiring that $\vec{s_1}$ belongs to the upper half-space.

The effective stress tensor is deduced from the total stress tensor by subtraction of the isotropic pore pressure tensor; therefore the orientations of the effective principal stresses $\vec{s_1}$, $\vec{s_2}$, $\vec{s_3}$ coincide with the orientations of the total principal stresses, and the magnitudes of the effective principal stresses $\sigma_1, \sigma_2, \sigma_3$ are deduced from the magnitudes of the total principal stresses by subtraction of the scalar pore pressure.

The matrix that transforms E into S is defined as S^E; its jth column represents the coordinates of $\vec{s_j}$ in the E frame. S^E is a rotation matrix and therefore depends on only three parameters. Choosing Euler's [1767] angles (θ, φ, ψ) as these parameters, this rotation is decomposed into three elementary rotations, of

respective angles θ, φ, and ψ and axes $\vec{e_3}$, $\vec{u_1}$, and $\vec{s_1}$ (Figure 2), and the matrix S^E can be expressed as

$$S^E = \begin{bmatrix} \sin\theta\sin\varphi & \cos\theta\cos\psi - \sin\theta\cos\varphi\sin\psi & -\cos\theta\sin\psi - \sin\theta\cos\varphi\cos\psi \\ -\cos\theta\sin\varphi & \sin\theta\cos\psi + \cos\theta\cos\varphi\sin\psi & -\sin\theta\sin\psi + \cos\theta\cos\varphi\cos\psi \\ \cos\varphi & \sin\varphi\sin\psi & \sin\varphi\cos\psi \end{bmatrix} \quad (3)$$

$\vec{s_1}$ depends only on two angles: θ and φ, while $\vec{s_2}$ and $\vec{s_3}$ require ψ. Finally, remembering that $\vec{s_1}$ is in the upper half-space, the following intervals of definition are obtained for each angle:

$$\theta \in [0, 2\pi[\ ;\ \varphi \in [0, \pi/2]\ ;\ \psi \in [0, 2\pi[\quad (4)$$

To facilitate the study, $\underline{\underline{T}}$ is decomposed in a fashion similar to that into pressure and deviatoric tensor, with the difference that tensional tensors must be avoided because of the friction law. Therefore the biggest isotropic tensor, $\sigma_3 \bullet \underline{\underline{I}}$, that still yields a compressive result is subtracted from $\underline{\underline{T}}$, and the result is scaled to 1 so as to define $\underline{\underline{T}}_d$:

$$\underline{\underline{T}}_d = \frac{1}{\sigma_1 - \sigma_3} \bullet [\underline{\underline{T}} - \sigma_3 \bullet \underline{\underline{I}}] \quad (5)$$

The shear and normal stress of these two tensors are related by

$$\vec{\tau} = (\sigma_1 - \sigma_3) \bullet \vec{\tau_d} \quad (6)$$

$$\vec{\sigma_n} = \sigma_3 \bullet \vec{e_3} + (\sigma_1 - \sigma_3) \bullet \vec{\sigma_{nd}} \quad (7)$$

σ_1, σ_2, σ_3 are also scaled by defining $s \in [0, +\infty[$ (equation (1)) and $\delta \in [0, 1]$ (equation (2)). The aspect ratio δ is also often more easily represented by θ_1 that can be graphically constructed (Figure 3) and that is defined as

$$\theta_1 = 2\,\mathrm{Arctan}(\sqrt{\delta}) \qquad \theta_1 \in [0, \pi/2] \quad (8)$$

$\underline{\underline{T}}_d$ is represented in the E frame by

$$T_d^E(\theta, \varphi, \psi, \delta) = S^E(\theta, \varphi, \psi) \bullet T_d^S(\delta) \bullet {}^tS^E(\theta, \varphi, \psi) \quad (9)$$

where

$$T_d^S = \begin{bmatrix} 1 & 0 & 0 \\ 0 & 1-\delta & 0 \\ 0 & 0 & 0 \end{bmatrix} \quad (10)$$

$\underline{\underline{T}}_d$ depends therefore on only four parameters: the orientation of the principal stresses (θ, φ, ψ) and the aspect ratio δ, yet it contains all the geometrical information about the shear stress (equation (6)). This can be easily understood because the Mohr's [1882] circles of $\underline{\underline{T}}_d$ (Figure 3b) are deduced from those of $\underline{\underline{T}}$ (Figure 3a) by a translation of $-\sigma_3$ along the σ_n axis and a similarity of ratio $1/(\sigma_1 - \sigma_3)$ centered on the origin and are

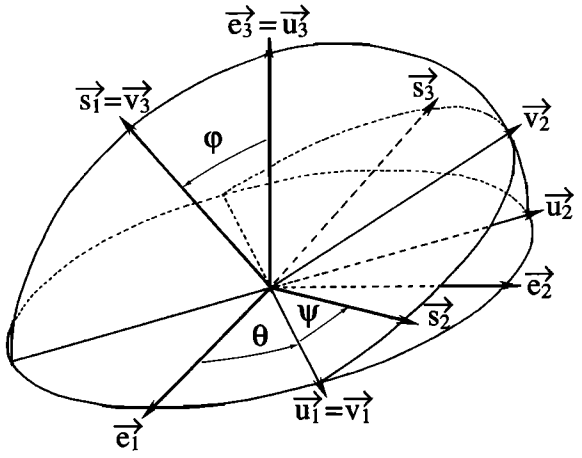

Fig. 2. Euler's [1767] angles. The fault plane frame $E = (\vec{e_1}, \vec{e_2}, \vec{e_3})$ is transformed into the principal stresses frame $S = (\vec{s_1}, \vec{s_2}, \vec{s_3})$ by three successive rotations of angle θ, φ, and ψ. The intermediate stages are $\vec{u_1}$, $\vec{u_2}$, $\vec{u_3}$ and $\vec{v_1}$, $\vec{v_2}$, $\vec{v_3}$.

therefore similar to those of $\underline{\underline{T}}$ and because these two tensors have the same eigenvectors, even though different eigenvalues. T^E can then be recovered from T_d^E by

$$T^E(\theta,\varphi,\psi,\sigma_1,s,\delta) = \sigma_1 \bullet (1-s) \bullet I + \sigma_1 \bullet s \bullet T_d^E(\theta,\varphi,\psi,\delta) \quad (11)$$

With the adopted sign convention, the stress $\vec{F}$ applied to the upper half-space of the fault plane is given by

$$\vec{F} = \underline{\underline{T}}(\vec{e_3}) \quad (12)$$

The normal stress $\vec{\sigma_n}$ and the shear stress $\vec{\tau}$ are then (Figure 1)

$$\vec{\sigma_n} = t_{33}^E \bullet \vec{e_3} \quad (13)$$

$$\vec{\tau} = t_{13}^E \bullet \vec{e_1} + t_{23}^E \bullet \vec{e_2} \quad (14)$$

Equations (12), (11), and (9) give the components of F^E as a function of $(\theta,\varphi,\psi,\sigma_1,\theta_1,s)$ (Table 2).

To apply the frictional constraint it is useful to define the scalar functions H and H_d as

$$H = \tau - \tan\varphi_0 \bullet \sigma_n \quad (15)$$

$$H_d = \tau_d - \tan\varphi_0 \bullet \sigma_{nd} \quad (16)$$

Defining the direct problem as that where the stress tensor $\underline{\underline{T}}$ is given and one looks for the orientation of the planes of failure and slip, $E = (\vec{e_1}, \vec{e_2}, \vec{e_3})$, with respect to the principal stresses frame, $S = (\vec{s_1}, \vec{s_2}, \vec{s_3})$, it is the inverse problem that is of interest in tectonics because the fault plane and slip are obtained from earthquake fault plane solution or structural

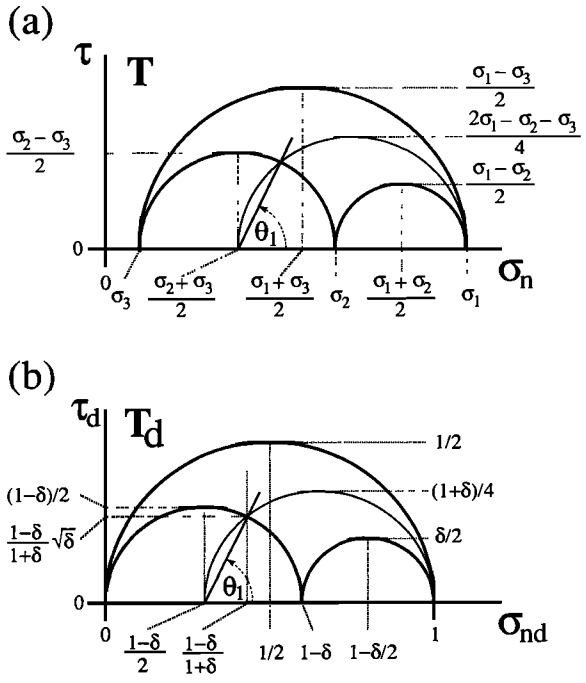

Fig. 3. Mohr's [1882] circles. To the classical outer and inner circles is added an intermediate circle that is centered on the σ_n axis and goes through the center of the left inner circle and through the point of coordinates $(\sigma_1,0)$. The angle θ_1 can be graphically constructed from the intersection of the left inner circle with that intermediate circle. (a) $\underline{\underline{T}}$. (b) $\underline{\underline{T}}_d$. The outer circle has diameter 1 and goes through the origin.

geology and the stress tensor is sought. This problem, when limited to one given plane of failure and slip, is by nature underdetermined, and its study aims only at describing the set of acceptable solutions.

THE GEOMETRICAL CONSTRAINT ALONE: VARIATIONS ON A THEME BY MCKENZIE [1969]

McKenzie [1969] showed that for stress tensors satisfying the geometrical constraint and when δ is fixed, the shear stress magnitude τ can be mapped as a function of the position of $\vec{s_1}$. Because the onset of slip is mechanically controlled by both shear, τ, and normal, σ_n, stress magnitudes, this mapping needs to be extended to σ_n and to the linear combination of τ and σ_n, H, that represents a friction law (equation (15)).

The derivation of analytical instead of numerical representation is emphasized because critical cases can then be associated with precise relationships between the parameters, relationships that can be physically interpreted. The emphasis on $\vec{s_1}$ is also relaxed so as to extend these maps to $\vec{s_2}$ and $\vec{s_3}$. Because using Euler's [1776] angles is a slightly different approach from that of McKenzie [1969], a preliminary task is to reformulate his results.

Formulation

The geometrical constraint is twofold:

1. The shear stress $\vec{\tau}$ on the fault plane must be parallel to the slip vector $\vec{e_1}$ [Wallace, 1951; Bott, 1959; McKenzie, 1969]. This can be expressed as (Figure 1 or equation (14))

$$t^E_{23} = 0 \tag{17}$$

2. The shear stress $\vec{\tau}$ and slip $\vec{e_1}$ must point in the same direction [McKenzie, 1969]:

$$t^E_{13} \geq 0 \tag{18}$$

$\underline{\underline{T}}$ depends on six parameters and is submitted to a linear constraint: the problem is then underdetermined and the set of solutions is the vectorial space of dimension five of the stress tensors whose matrices in E, T^E, satisfy $t^E_{23} = 0$. The general solution is then

$$T^E = \begin{bmatrix} t^E_{11} & t^E_{12} & t^E_{13} \\ t^E_{12} & t^E_{22} & 0 \\ t^E_{13} & 0 & t^E_{33} \end{bmatrix} \tag{19}$$

where the t^E_{ij} are arbitrary. This vectorial space structure can be used to reduce the problem in two ways [Carey and Brunier, 1974; Angelier, 1975]. First, because any isotropic tensor $\alpha\underline{I}$ belongs to that space, as one would expect since in that case, $\vec{\tau} = \vec{0}$, it can be added to any solution to produce another solution. Second, a scaling factor on $\underline{\underline{T}}$ will not modify the problem. Therefore the general solution can be written as

$$\underline{\underline{T}}(\theta,\varphi,\psi,\sigma_1,s,\delta) = \sigma_1 \bullet (1\text{-}s) \bullet \underline{I} + \sigma_1 \bullet s \bullet \underline{\underline{T}}_d(\theta,\varphi,\psi,\delta) \tag{20}$$

where σ_1 and s are arbitrary and $\underline{\underline{T}}_d$ satisfies the geometrical constraint (equations (17) and (18)).

TABLE 2. Components of the Stress Applied to the Fault Plane

Component		Value
t^E_{13}	=	$\sigma_1 \bullet s \bullet t^E_{d13}$
t^E_{23}	=	$\sigma_1 \bullet s \bullet t^E_{d23}$
t^E_{33}	=	$\sigma_3 + \sigma_1 \bullet s \bullet t^E_{d33}$
t^E_{d13}	=	$\frac{\sin\varphi}{1+\cos\theta_1} \bullet [(1+\cos\theta_1\cos2\psi)\cos\varphi\sin\theta + \cos\theta_1\sin2\psi\cos\theta]$
t^E_{d23}	=	$\frac{-\sin\varphi}{1+\cos\theta_1} \bullet [(1+\cos\theta_1\cos2\psi)\cos\varphi\cos\theta - \cos\theta_1\sin2\psi\sin\theta]$
t^E_{d33}	=	$1-\frac{\sin^2\varphi}{1+\cos\theta_1} \bullet (1+\cos\theta_1\cos2\psi)$

Therefore only $\underline{\underline{T}}_d$ needs to be studied. This can be independently derived either by noticing that $\underline{\underline{T}}$ and $\underline{\underline{T}}_d$ have parallel shear stress (equation (6)) or by noticing that the orientation of $\vec{\tau}$, i.e., the ratio t^E_{23}/t^E_{13}, depends only on θ, φ, ψ and δ (Table 2). The dependence on δ of that orientation is the essence of Bott's [1959] contribution. The only relevant parameters to this study are therefore θ, φ, ψ, and δ; σ_1 and s remain unconstrained.

Sign and Zeros of t^E_{d23}

Because of symmetries, the study is limited to $\theta \in [0,\pi]$; $\varphi \in [0, \pi/2]$; $\psi \in [0, 2\pi]$; two particular cases where t^E_{d23} does not depend on ψ are distinguished from the general case.

Particular case 1. If $\delta = 1$, then $\sigma_2 = \sigma_3$ and $\theta_1 = \pi/2$, and $t^E_{d23} = 0$ if and only if $\varphi = 0$ or $\varphi = \pi/2$ or $\theta = \pi/2$; ψ remains a free parameter.

Particular case 2. If $\vec{s_1} // \vec{e_2}$, then $\varphi = \pi/2$ and $\theta = 0$ and $t^E_{d23} = 0$ regardless of the value of ψ.

General case. If $\delta \neq 1$ and $\vec{s_1} \times \vec{e_2} \neq \vec{0}$, the functions

$$K(\theta,\varphi) = \frac{\cos\varphi\cos\theta}{\sqrt{1-\sin^2\varphi\cos^2\theta}} \tag{21}$$

$$\chi(\theta,\varphi) = \mathrm{Arcsin}[K(\theta,\varphi)] \tag{22}$$

are then defined and

$$t^E_{d23} = \frac{\cos\theta_1}{1+\cos\theta_1} \bullet \sin\varphi \bullet \sqrt{1-\sin^2\varphi\cos^2\theta} \bullet [\sin(2\psi-\chi) - \frac{K}{\cos\theta_1}] \tag{23}$$

Except when $\varphi = 0$ ($\vec{s_1} = \vec{e_3}$), in which case $t^E_{d23} = 0$, the sign and zeros of t^E_{d23} are the same as those of f defined as

$$f(\theta,\varphi,\psi,\theta_1) = \sin[2\psi-\chi(\theta,\varphi)] - K(\theta,\varphi)/\cos\theta_1 \tag{24}$$

Three regions in the (θ,φ) plane can then be distinguished (Figure 4a): (1) a region R^+ where $K < -\cos\theta_1$ and then for any value of ψ, $t^E_{d23} > 0$; (2) a region R^- where $K > \cos\theta_1$ and then for any value of ψ, $t^E_{d23} < 0$; and (3) a region R^0 where $-\cos\theta_1 < K < \cos\theta_1$; in that region the sign of t^E_{d23} depends on ψ once θ and φ are fixed, and it is always possible to find ψ so that $t^E_{d23} = 0$; the only possible choices for that are ψ_1 and ψ_2:

$$\psi_1(\theta,\varphi,\delta) = \frac{\chi(\theta,\varphi)}{2} + \frac{1}{2} \bullet \mathrm{Arcsin}[\frac{K(\theta,\varphi)}{\cos\theta_1}] \tag{25}$$

$$\psi_2(\theta,\varphi,\delta) = \frac{\chi(\theta,\varphi)}{2} + \frac{\pi}{2} - \frac{1}{2} \bullet \mathrm{Arcsin}[\frac{K(\theta,\varphi)}{\cos\theta_1}] \tag{26}$$

Discussion

C(α) is defined as the great circle that passes through A_2 and whose plane is at angle α with $\vec{e_3}$ (Figure 4b). Its equation, i.e., the condition for $\vec{s_1}$ to be on that circle, is

$$\sin\theta = \tan\alpha / \tan\varphi \tag{27}$$

D(α) is the curve (Figure 4b) defined by

$$K^2(\theta,\varphi) = \cos^2\alpha \tag{28}$$

The boundary between the three regions R^-, R^0, and R^+ as defined before is $D(\theta_1)$. When $\vec{s_1}$ describes $D(\theta_1)$, the two stress tensor solutions of the geometrical constraint coincide because $\psi_1(\theta,\varphi,\delta) = \psi_2(\theta,\varphi,\delta)$. Therefore $\vec{s_2}$ and $\vec{s_3}$ also describe single curves that are defined as $D''(\theta_1)$ and $D'''(\theta_1)$.

In the general case, for a stress tensor solution of $t^E_{d23} = 0$, ψ is either $\psi_1(\theta,\varphi,\delta)$ or $\psi_2(\theta,\varphi,\delta)$ and can then be eliminated from the expression of stress components of Table 2. The resulting expression of a component, t, that can be either τ_d, σ_{nd}, or H_d are of the type (Table 3)

$$t(\theta,\varphi,\delta,\varepsilon) = A(\theta,\varphi) \bullet N(\theta,\varphi,\delta,\varepsilon) + B \tag{29}$$

where $\varepsilon + 1$ if ψ_1 has been substituted and $\varepsilon = -1$ if ψ_2 has been substituted. The corresponding functions will be designated as t^+ (case $\varepsilon = +1$) and t^- (case $\varepsilon = -1$). The shear component $t^E_{d13}(\theta,\varphi,\delta,\varepsilon)$ is obviously positive (Table 3) in the domain of study: $\theta \in [0,\pi]$ and $\varphi \in [0,\pi/2]$. By symmetry it is negative in the other quadrant $\theta \in [0,-\pi]$, $\varphi \in [0,\pi/2]$. Therefore, once the first geometrical condition $t^E_{d23} = 0$ is satisfied, the second condition $t^E_{d13} \geq 0$ is satisfied if and only if $\vec{s_1}$ belongs to the dilatational quadrant. The vector $\vec{s_1}$ is then restricted to the region R_G that is the intersection of the R^0 region with the dilatational quadrant; this region is bounded by the fault plane and $D(\theta_1)$ and depends only on δ (Figure 4c).

There are then only five cases where $t^E_{d23} = 0$ [McKenzie, 1969]:

1. $\underline{\underline{T}}$ is isotropic: $\sigma_1 = \sigma_2 = \sigma_3$.
2. $\underline{\underline{T}}$ is degenerate with $\sigma_2 = \sigma_3$ ($\delta = 1$), and $\vec{s_1}$ belongs either to the $(\vec{e_1}, \vec{e_3})$ plane (P, T plane) or to the $(\vec{e_1}, \vec{e_2})$ plane (fault plane).
3. The vector $\vec{s_1}$ is along the B axis: $\vec{s_1} = \vec{e_2}$.
4. The vector $\vec{s_1}$ is normal to the fault plane: $\vec{s_1} = \vec{e_3}$.
5. The vector $\vec{s_1}$ belongs to R_G region, and the orientation of $(\vec{s_2}, \vec{s_3})$ is defined by either $\psi_1(\theta,\varphi,\delta)$ or $\psi_2(\theta,\varphi,\delta)$. The general solution is then

$$\underline{\underline{T}}(\theta,\varphi,\psi,\sigma_1,s,\delta) = \sigma_1 \bullet (1-s) \bullet \underline{\underline{I}} + \sigma_1 \bullet s \bullet \underline{\underline{T}}_d(\theta,\varphi,\psi=\psi_1 \text{ or } \psi_2,\delta) \tag{30}$$

where σ_1 and s are arbitrary and $(\theta,\varphi) \in R_G$. The R_G region includes the positions of $\vec{s_1}$ obtained in cases 3 and 4 and its definition can be extended to include case 2. The general case can then be extended to include all the particular cases if one keeps in mind that in these cases ψ remains unconstrained.

Maps of the Stress Components

For $\underline{\underline{T}}_d$ satisfying the geometrical constraint and once δ and ε are fixed, the magnitude $t(\theta,\varphi,\delta,\varepsilon)$ (equation 29 and Table 3) of either τ_d, σ_{nd}, or H_d depends only on (θ,φ) which in turn

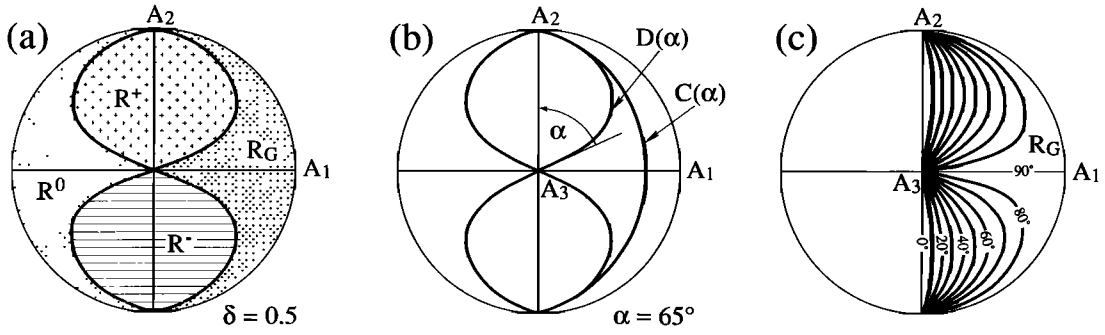

Fig. 4. (a) R^- (lined area), R^0 (dotted area) and R^+ (pluses) regions for $\vec{s_1}$. The upper half sphere ($x_3 \geq 0$) is projected into the fault plane defined by $(\vec{e_1}, \vec{e_2})$ by an azimuthal equal-area projection [Lambert, 1772]; $\vec{s_1}$ represents any couple (θ,φ). The boundary between these three regions is the curve $D(\theta_1)$. R_G (thicker dots) is the dilatational part, i.e., the right side, of R^0. (b) $C(\alpha)$ and $D(\alpha)$. $C(\alpha)$ is the great circle at angle α from $\vec{e_3}$ that passes through A_2. $D(\alpha)$ is the locus of $\vec{s_1}$ satisfying equation (28). The projection of $D(\alpha)$ is tangent to the projection of $C(\alpha)$ at A_2 and to the line at angle a from A_3A_2 at A_2. (c) R_G regions for $\theta_1 = 0°$ to $90°$ by increment of $10°$.

determines the position of $\vec{s_1}$, $\vec{s_2}$ or $\vec{s_3}$ through equations (3) and (25) or (26). In other words, the value of t can be mapped as a function of the position of either $\vec{s_1}$ or $\vec{s_2}$ or $\vec{s_3}$. Such maps for $\underline{\underline{T}}_d$ can be transferred to $\underline{\underline{T}}$ through equations (6) and (7). To draw the V_0 level curve of such maps requires to solve for either θ or φ the equation

$$A(\theta, \varphi) \bullet N(\theta, \varphi, \theta_1, \varepsilon) + B = V_0 \qquad (31)$$

TABLE 3. Components of the Stress Applied to the Fault Plane when $\vec{\tau} // \vec{e_1}$

Function		Definition		Value	B
			Shear stress		
τ	=	t^E_{13}	=	$\sigma_1 \bullet s \bullet A_\tau \bullet N$	
τ_d	=	$t^E_{d13} = \tau/(\sigma_1-\sigma_3)$	=	$A_\tau \bullet N$	$B_\tau = 0$
τ_*	=	$2\tau_d$	=	$2 \bullet A_\tau \bullet N$	
			Normal stress		
σ_n	=	t^E_{33}	=	$\sigma_1 \bullet (1 + s \bullet A_\sigma \bullet N)$	
σ_{nd}	=	$t^E_{d33} = \dfrac{\sigma_n - \sigma_3}{\sigma_1 - \sigma_3}$	=	$1 + A_\sigma \bullet N$	$B_\sigma = 1$
σ_{n*}	=	σ_{nd}	=	$1 + A_\sigma \bullet N$	
			Friction law		
H	=	$\tau - \tan\varphi_0 \bullet \sigma_n$	=	$\sigma_1 \bullet (s \bullet A_H \bullet N - \tan\varphi_0)$	
H_d	=	$\tau_d - \tan\varphi_0 \bullet \sigma_{nd}$	=	$A_H \bullet N - \tan\varphi_0$	$B_H = -\tan\varphi_0$
H_*	=	$2 \bullet (H_d + \tan\varphi_0)/\tan\varphi_1$	=	$2 \bullet A_H \bullet N/\tan\varphi_1$	

Function		Expression in (θ,ϕ)		Expression in (θ,α)
R_D	=	$\sqrt{1 - \cos^2\varphi \dfrac{\tan^2\theta_1}{\tan^2\theta}}$	=	$\sqrt{\dfrac{1 - \cos^2\alpha\cos^2\theta/\cos^2\theta_1}{1 - \cos^2\alpha\cos^2\theta}}$
N	=	$\dfrac{1 + \varepsilon\cos\theta_1 R_D(\theta,\varphi,\theta_1)}{1 + \cos\theta_1}$	=	$\dfrac{1 + \varepsilon\cos\theta_1 R_D(\theta,\alpha,\theta_1)}{1 + \cos\theta_1}$
A_τ	=	$\dfrac{1}{2}\dfrac{\sin2\varphi\sin\theta}{1 - \sin^2\varphi\cos^2\theta}$	=	$\dfrac{1}{2}\sin2\alpha$
A_σ	=	$-\dfrac{\sin^2\varphi\sin^2\theta}{1 - \sin^2\varphi\cos^2\theta}$	=	$-\sin^2\alpha$
A_H	=	$\dfrac{\sin\theta\sin\varphi[\cos\varphi + \tan\varphi_0\sin\varphi\sin\theta]}{1 - \sin^2\varphi\cos^2\theta}$	=	$\dfrac{\sin(2\alpha-\varphi_0) + \sin\varphi_0}{2\cos\varphi_0}$

Analytical solutions can be found by noticing that the circles $C(\alpha)$ are the level curves of the function $A(\theta,\varphi)$. Replacing then (θ,φ) by (θ,α) (Table 3) where α is defined as in equation (27) leads to

$$A(\alpha) \bullet N(\theta, \alpha, \theta_1, \varepsilon) + B = V_0 \qquad (32)$$

that can be solved in α, thereby allowing a parametric representation of the solutions: $\theta(\alpha)$, $\varphi(\alpha)$. A full discussion of this method and the results concerning the variations and level curves of τ_d, σ_{nd}, or H_d is given by Célérier [1987].

As an example, the maps for $\delta = 0.3$ are shown in Figure 5 where the function t is normalized into t_* as defined in Table 3 so that the absolute minimum is 0 and the absolute maximum 1. The values and locations of the extrema are given in Table 4. These level curves correspond in the (σ_n,τ) plane to the part of the line $t = V_0$ that is between the inner and outer Mohr's [1882] circles, and all the critical cases through which the

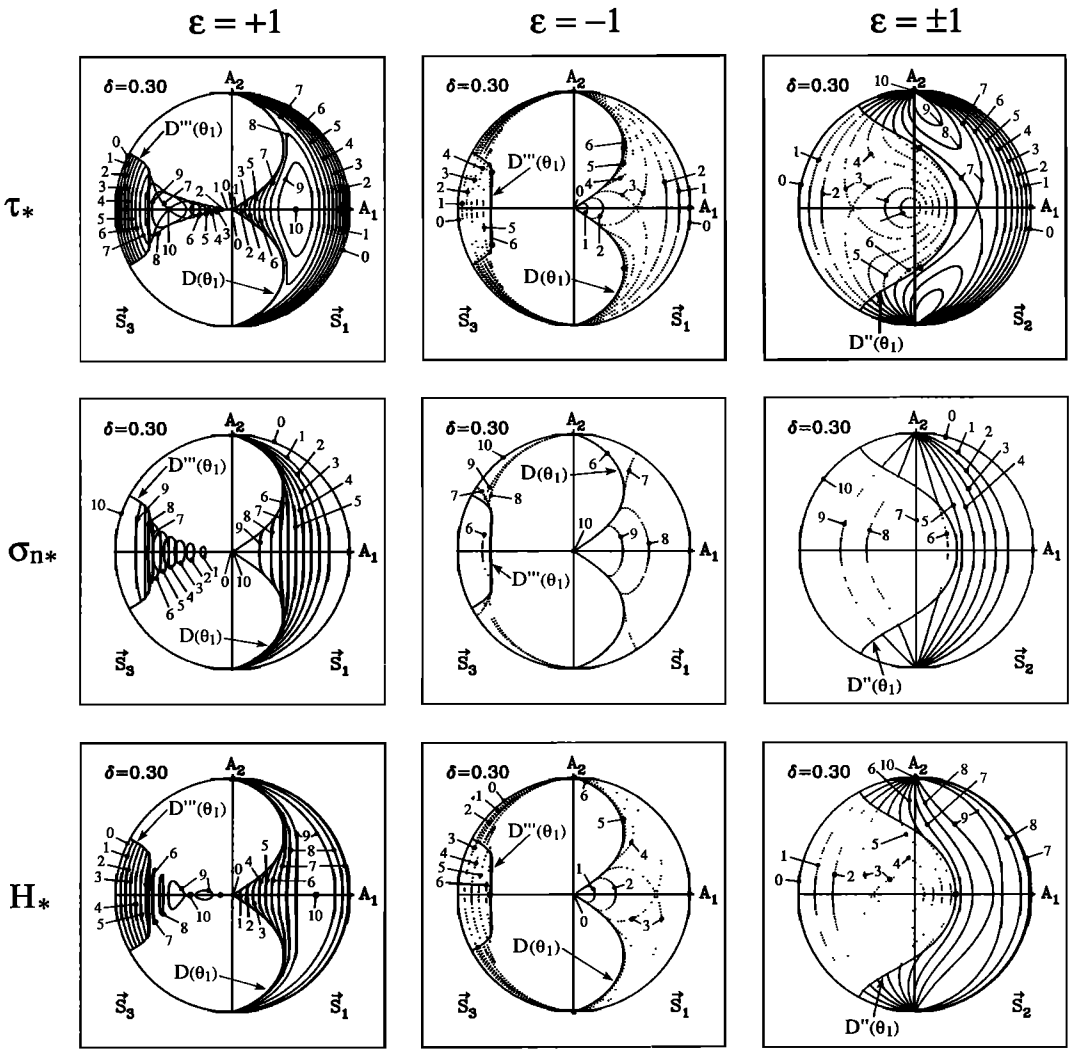

Fig. 5. Maps of stress components t_* for $\delta = 0.3$. Using the same equal-area projection as in Figure 4, the 11 level curves, from $t_* = 0$ to $t_* = 1$ by increment of 1/10, are labeled from 0 to 10 in that order. (Top) τ_*, (middle) σ_{n*}, (bottom) H_*. (Left) $\vec{s_1}$ (in the dilatational quadrant) and $\vec{s_3}$ (in the compressional quadrant) trajectories for ε - +1 (solid curves); (center) $\vec{s_1}$, $\vec{s_3}$ trajectories for $\varepsilon = -1$ (dotted curves); (right) $\vec{s_2}$ trajectories for both $\varepsilon = +1$ (solid curves) and $\varepsilon = -1$ (dotted curves). The curves $D(\theta_1)$, $D''(\theta_1)$, and $D'''(\theta_1)$ are shown in solid curve (best seen among the dotted trajectories for $\vec{s_3}$, and clearly crosscutting the level for $\vec{s_2}$ at the location where dotted and continuous curves connect). The locations of the maxima of t_*^+ and t_*^- are marked by isolated thick points. There are less than 11 level curves for t_*^- because it does not span the whole range between 0 and 1 (Table 4). Note that the P (P_f) axis is a saddle point for the $\vec{s_1}$ levels of τ_*^- (H_*^-) and a summit for those of τ_*^+ (H_*^+).

TABLE 4. Absolute Extrema

Function	Case	Maximum			Minimum		
		Value	Location of $\vec{s_1}$		Value	Location of $\vec{s_1}$	
τ_*^+		1	P	[$\alpha=\pi/4$]	0	A_3;$C(\pi/2)$	[$\alpha=0;\pi/2$]
σ_{n*}^+		1	A_3	[$\alpha=0$]	0	$C(\pi/2)$	[$\alpha=\pi/2$]
H_*^+		1	P_f	[$\alpha=\varphi_1$]	0	A_3	[$\alpha=0$]
τ_*^-	$\theta_1\le\pi/4$	$2\sqrt{\delta(1-\delta)/(1+\delta)}$	A_2	[$\alpha=\theta_1$]	0	A_3;$C(\pi/2)$	[$\alpha=0;\pi/2$]
τ_*^-	$\theta_1\ge\pi/4$	$(1+\delta)/2$	$D(\theta_1)$	[$\alpha=\pi/4$]	0	A_3;$C(\pi/2)$	[$\alpha=0;\pi/2$]
σ_{n*}^-		1	A_3	[$\alpha=0$]	$(1-\delta)/(1+\delta)$	A_2	[$\alpha=\theta_1$]
H_*^-	$\theta_1\le\varphi_1$	$s_c\sqrt{\delta}\cos(\theta_1-\varphi_0)/\sin\varphi_0$	A_2	[$\alpha=\theta_1$]	0	A_3	[$\alpha=0$]
H_*^-	$\theta_1\ge\varphi_1$	$(1+\delta)/2$	$D(\theta_1)$	[$\alpha=\varphi_1$]	0	A_3	[$\alpha=0$]

positive and negative superscript correspond to $\varepsilon = +1$ and to $\varepsilon = -1$, respectively.

curves change shape correspond to the tangence of that line $t = V_0$ with one of Mohr's circle. The t^+ and t^- level curves connect on $D(\theta_1)$, $D''(\theta_1)$, and $D'''(\theta_1)$ for $\vec{s_1}$, $\vec{s_2}$, and $\vec{s_3}$, respectively. This corresponds in the (σ_n,τ) plane to the circle that has the σ_n axis as diameter and passes through σ_1 and $(\sigma_2+\sigma_3)/2$ (i.e., 1 and $(1+\delta)/2$ for $\underline{\underline{T}}_d$) on that axis (Figure 3). The $\vec{s_1}$ maps for t^+ and t^- cover the same domain R_G. The $\vec{s_2}$ maps for t^+ and t^- cover different domains separated by $D''(\theta_1)$ and whose reunion is the whole space. The $\vec{s_3}$ maps are included in the compressional quadrant, and the reunion of the t^+ and t^- domain covers the area between the fault plane and $D(\theta_2)$, where

$$\theta_2 = 2\,\mathrm{Arctan}(\sqrt{1-\delta}) \tag{33}$$

This reflects that the symmetry between $\vec{s_1}$ and $\vec{s_3}$ corresponds to that between δ and $1-\delta$. The $\vec{s_1}$ maps for τ_* and H_* display the difference between the $\varepsilon = +1$ and the $\varepsilon = -1$ case: τ_*^+ and H_*^+ reach their maximum, 1, in P and a position that is defined as P_f, respectively, and the whole map represent a hill around that point; τ_*^- and H_*^- reach theirs, which is smaller than 1 (Table 4), either in A_2 (as H in the case $\delta = 0.3$) or inside $D(\theta_1)$ (as τ in the case $\delta = 0.3$), and the P or P_f location corresponds to a saddle point. Also τ_*^+ and τ_*^- reach their minimum, zero, either in A_3 or on $C(\pi/2)$, whereas H_*^+ and H_*^- reach it only in A_3.

Conclusions

1. The geometrical constraint constrains only $\underline{\underline{T}}_d$; hence, it constrains only the orientation of $\vec{s_1}$, $\vec{s_2}$, $\vec{s_3}$ and δ.

2. When δ is fixed and the geometrical constraint is satisfied, $\vec{s_1}$ belongs to the R_G region, $\vec{s_3}$ belongs to the region within the compressional quadrant that is bounded by the fault plane and $D(\theta_2)$ where θ_2 corresponds to $1-\delta$ (equation (33)), and $\vec{s_2}$ can have any orientation in space (Figure 5).

3. If δ is not known, the union of all the R_G regions for all possible δ values adds up to the whole dilatational quadrant (Figure 4c): $\vec{s_1}$ can therefore lie anywhere in it [McKenzie, 1969]. This sole result can be demonstrated much more rapidly by noticing that the scalar products $\vec{s_1} \bullet \vec{e_3}$ and $\vec{s_1} \bullet \vec{\tau}$ have same sign [Angelier and Mechler, 1977]. For each position of $\vec{s_1}$ within that dilatational quadrant, a whole range or orientations of $(\vec{s_2}, \vec{s_3})$ that correspond to the δ dependence of ψ_1 and ψ_2 is allowed.

4. If δ is fixed, the magnitude of τ_{d*}, σ_{nd*}, and H_{d*} can be mapped as a function of the position of $\vec{s_1}$, $\vec{s_2}$, and $\vec{s_3}$ (Figure 5). Two cases ($\varepsilon = +1$ and $\varepsilon = -1$) must be distinguished.

MECHANICAL CONSTRAINT

Although this paper concentrates on frictional sliding on a preexisting plane of weakness, it is useful to briefly review the constraint on stress tensor for failure in intact rocks.

Failure

Coulomb's [1776] failure criterion assumes that the failure envelope [Mohr, 1900] is a straight line in Mohr's [1882] (σ_n, τ) plane (Figure 6a)[Handin, 1969; Jaeger and Cook, 1979]:

$$\tau = \tau_0 + \tan\varphi_0 \bullet \sigma_n \tag{34}$$

where φ_0 is the angle of internal friction and τ_0 is the cohesive shear stress. Even though experiments have shown that the failure envelope is concave [Byerlee, 1967], this linear approximation remains acceptable within limited stress ranges and attractive because of its simplicity.

Failure occurs when there is a plane orientation for which the state of stress corresponds to the failure criterion (equation (34)); therefore it occurs when the outer Mohr's [1882] circle is tangent to the straight line representing that failure criterion (Figure 6a). For any point on this outer circle, $\vec{s_2}$ is within the fault plane; therefore

$$\vec{s_2} \perp \vec{e_3} \tag{35}$$

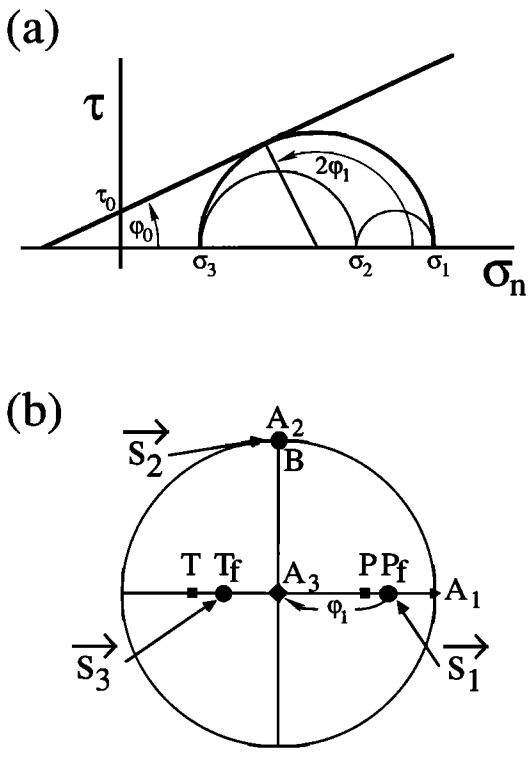

Fig. 6. Coulomb [1776] failure. (a) Mohr's circles. (b) Orientations of the principal stresses in projection. Using seismological terminology, A_2 is the B axis, the fault plane is horizontal, the second nodal plane is the vertical plane that contains B, and P and T are at 45° from these two planes [Scheidegger, 1964]. The positions of $\vec{s_1}$ and $\vec{s_3}$ at failure are defined as P_f and T_f.

The tangence implies first that the angle φ_1 between the fault plane normal $\vec{e_3}$ and $\vec{s_1}$ is

$$\varphi_1 = \varphi_0/2 + \pi/4 \tag{36}$$

and second that the parameter s' defined as

$$s' = \frac{\sigma_1 - \sigma_3}{\sigma_1 + \tau_0/\tan\varphi_0} \tag{37}$$

has reached a critical value s_c that depends only on φ_0:

$$s_c = \frac{2\sin\varphi_0}{1+\sin\varphi_0} = \frac{2\tan\varphi_0}{\tan\varphi_1} \tag{38}$$

so that

$$s' = s_c \tag{39}$$

Finally, the slip vector $\vec{e_1}$ must be parallel to the shear stress on the fault plane [Wallace, 1951; Bott, 1959; McKenzie, 1969], so that

$$\vec{e_1} \perp \vec{s_2} \tag{40}$$

Equations (35) and (36) define two conjugate fault planes and are the basis of Anderson's [1951] theory of faulting; equation (40) defines the orientation of the slip within each of these fault planes; equation (39) indicates the relative level of stress necessary to cause failure.

Starting from the fault plane and slip vector $\vec{e_1}$ the four former constraints uniquely define the orientations of the principal stresses at failure: $\vec{s_1}$, $\vec{s_2}$, $\vec{s_3}$ are in positions that we define as P_f, B, T_f, respectively (Figure 6b). The P_f axis is always closer to the slip vector $\vec{e_1}$ than the P axis. Also s' must be equal to s_c. The parameter s' and the orientations of the principal stresses are all the information that can be derived about the stress tensor. Neither σ_2, which does not play any role in this theory, nor the absolute magnitudes of the principal stresses can be evaluated. Finally, two problems may be encountered if one tries to apply these results to fault plane solutions: (1) because the angle of internal friction, φ_0, depends on the rock type, if the rocks that failed are not known, the orientations of $\vec{s_1}$ and $\vec{s_3}$ and the values of s' will be poorly constrained; and (2) it will often be difficult to distinguish the auxiliary plane from the fault plane.

In seismology the P, B, and T axes are assumed to represent the positions of $\vec{s_1}$, $\vec{s_2}$, $\vec{s_3}$ because they display enough spatial regularity and probably also because they do not necessitate to distinguish the fault plane from the other nodal plane [Honda and Masatuka, 1952; Scheidegger, 1964]. However, this correspond to a maximum shear stress failure criterion which, if reasonable for metals [Tresca, 1868], is unrealistic for crustal rocks [Wallace, 1951; Jaeger and Cook, 1979].

Friction

Equation (34) has been shown to describe frictional sliding [Amontons, 1699; Coulomb, 1776] before it was used to study failure and hereto remains the basic law of friction [Palmer, 1949; Rabinowicz, 1963]. This law adequately represent the failure of rocks on a preexisting plane of weakness, but it applies to the plane of weakness only, as opposed to any plane as in the case of failure [Talobre, 1957; Jaeger, 1959]. This results in three significant differences:

1. The parameter φ_0 is now the angle of external friction, which is generally much smaller than the angle of internal friction.
2. The cohesion τ_0 has also usually a smaller value than for failure.
3. The contact between the friction line representing equation (34) in the (σ_n, τ) plane does not necessarily occur on the outer Mohr's circle but generally below it, so that $\vec{s_2}$ is not necessarily parallel to the fault plane.

As a consequence of differences 1 and 2, friction on a plane of weakness is likely to occur before a state of stress high enough to cause failure is reached; as expressed by difference 3 the orientation of the stresses and of the fault plane are not tightly related since the latter one is not, as in the case of

failure, a consequence of the former [Wallace, 1951; Talobre, 1957; Bott, 1959; Jaeger, 1960; Donath, 1964; Handin, 1969; McKenzie, 1969].

The friction law holds only if the normal stress is compressive:

$$\sigma_n > 0 \tag{41}$$

which is guaranteed for all plane orientations as long as

$$\sigma_3 > 0 \text{ or } s < 1 \tag{42}$$

There are, however, two aspects that are simpler in the case of friction: (1) actual measurements show this linear relationship to be accurate [Byerlee, 1967], and (2) at relatively high stresses ($\sigma_3 > 50$ bars or depth > 300 m if the pore pressure is hydrostatic) the coefficients τ_0 and φ_0 for maximum friction are fairly independent of the rock type except for clays [Byerlee, 1978]:

$$\varphi_0 = 40.4° \quad \text{and} \quad \tau_0 = 0 \quad \text{if} \quad \sigma_n \le 200 \text{ MPa} \tag{43}$$

$$\varphi_0 = 31° \quad \text{and} \quad \tau_0 = 60 \text{ MPa} \quad \text{if} \quad \sigma_n \ge 200 \text{ MPa} \tag{44}$$

In situ stress measurements are consistent with these laboratory results [Brace and Kohlstedt, 1980; Zoback and Healy, 1984].

Remarks

The fundamental difference between the two processes described above is not as much that between failure and friction, as that between isotropic and anisotropic material [Talobre, 1957; Jaeger and Cook, 1979].

Also, the study of a Coulomb's [1776] law can be reduced to the case $\tau_0 = 0$ since if $\underline{\underline{T}}$ satisfies equation (34) then $\underline{\underline{T}}'$ defined as

$$\underline{\underline{T}}' = \underline{\underline{T}} + \frac{\tau_0}{\tan\varphi_0} \bullet \underline{\underline{I}} \tag{45}$$

satisfies the same constraint where $\tau_0 = 0$ [Jaeger and Rosengren, 1969].

In the case of friction, only two-dimensional problems [Talobre, 1957; Jaeger, 1959, 1960, 1962, 1971; Donath, 1964; Raleigh et al., 1972; Jaeger and Cook, 1979] and three-dimensional direct problems [Wallace, 1951; Bott, 1959; Jaeger and Rosengren,1969] have been studied.

THE THREE-DIMENSIONAL INVERSE PROBLEM WITH GEOMETRICAL AND FRICTIONAL CONSTRAINTS TOGETHER

Reduction

For $\underline{\underline{T}}$ to satisfy the friction law (equation (34)) and the geometrical constraint (equations (17) and (18)) it is necessary and sufficient that $\underline{\underline{T}}'$ as defined in equation (45) satisfies the same constraints with $\tau_0 = 0$. We will therefore henceforth limit our study to the case $\tau_0 = 0$. Since in real situations τ_0 is small compared to σ_1, the results can be directly applied. However, if τ_0 is not negligible, it is sufficient to substitute in all what follows $\underline{\underline{T}}'$ for $\underline{\underline{T}}$ and s' for s with

$$s' = (\sigma_1' - \sigma_3')/\sigma_1' = (\sigma_1 - \sigma_3)/(\sigma_1 + \tau_0/\tan\varphi_0) \tag{46}$$

In other terms the discussion for $\tau_0 = 0$ can be extended to $\tau_0 \neq 0$ simply by changing the definition of s originally given in equation (1) into the one given later in equation (37).

Formulation

Applying the frictional constraint (equation (34)) on the fault plane when the geometrical constraint (equations (17) and (18)) is already satisfied and when $\tau_0 = 0$ yields

$$H = t^E_{13} - \tan\varphi_0 \bullet t^E_{33} = 0 \tag{47}$$

or

$$H_d = t^E_{d13} - \tan\varphi_0 \bullet t^E_{d33} = (1/s - 1) \bullet \tan\varphi_0 \tag{48}$$

The set of solutions is a vectorial space of dimension 4:

$$T^E = \begin{bmatrix} t^E_{11} & t^E_{12} & \tan\varphi_0 \bullet t^E_{33} \\ t^E_{12} & t^E_{22} & 0 \\ \tan\varphi_0 \bullet t^E_{33} & 0 & t^E_{33} \end{bmatrix} \tag{49}$$

where the t^E_{ij} are arbitrary. This time, isotropic tensors, $\alpha\underline{\underline{I}}$, are not solutions because of the frictional constraint. If we consider the decomposition of $\underline{\underline{T}}$ into $\underline{\underline{I}}$ and $\underline{\underline{T}}_d$, the general solution is

$$\underline{\underline{T}}(\theta,\varphi,\psi,\sigma_1,\delta) = \sigma_1 \bullet (1-s) \bullet \underline{\underline{I}} + \sigma_1 \bullet s \bullet \underline{\underline{T}}_d(\theta,\varphi,\psi=\psi_1 \text{ or } \psi_2,\delta) \tag{50}$$

with the only three requirements that (1) $(\theta,\varphi) \in R_G$; (2) either $\psi_1(\theta,\varphi,\delta)$ or $\psi_2(\theta,\varphi,\delta)$ have been substituted for ψ in $\underline{\underline{T}}_d(\theta,\varphi,\psi,\delta)$; and (3) $\underline{\underline{T}}_d(\theta,\varphi,\delta)$ satisfies the frictional constraint (equation (48)). Because of requirements 1 and 2, $\underline{\underline{T}}_d(\theta,\varphi,\delta)$ already satisfies the geometrical constraint; it is therefore sufficient to find $\underline{\underline{T}}_d(\theta,\varphi,\delta)$ that satisfies requirement 3.

Because the two constraints (equations (17) and (34)) are homogeneous, a scaling factor on the magnitudes of the principal stresses does not affect the problem; this can be seen in equation (49) where the t^E_{ij} can be multiplied by any constant or in equation (50) where σ_1 remains unconstrained. There are then five relevant parameters to this problem: $(\theta,\varphi,\psi,s,\delta)$ and two constraints: equations (17) and (34). The number of degree of freedom is then not reduced compared to the geometrical constraint alone because adding the new frictional constraint requires the addition of a new parameter: s. Therefore we can only expect to express two parameters as a function of the three

others. We can then express φ and ψ as a function of θ, s, and δ; this implies that once s and δ are fixed, $\vec{s_1}$, $\vec{s_2}$, $\vec{s_3}$ will each describe a trajectory parameterized by θ. There is then a relationship between magnitudes (i.e., s, δ) and orientations (i.e., θ, φ, ψ). We will describe this relationship by discussing the shape of these trajectories as a function of (s, δ).

Once the geometrical constraint is satisfied, H_d is a function of $(\theta,\varphi,\delta,\varepsilon)$ only (Table 3). Using H_*, that is, a normalized version of H_d (Table 3), the frictional constraint (equation (48)) becomes

$$H_*(\theta,\varphi,\delta,\varepsilon) = s_c/s \tag{51}$$

where s_c is as in equation (38). In what follows the figures are drawn for $\varphi_0 = 31°$ (equation (44)) and therefore

$$s_c = 0.679 \tag{52}$$

This formulation has the advantage on equation (47) that s is already separated from the three other parameters (θ,φ,δ) and shows that if s and δ are fixed, then $\vec{s_1}$, $\vec{s_2}$, $\vec{s_3}$ must be on the trajectories that correspond to the H level curve $H_* = V_0$ with

$$V_0 = s_c/s \tag{53}$$

The study of the level curves of H_* shows [Célérier, 1987] that the whole discussion can be done in Mohr's [1882] domain (Figure 7). The figure depends on only two parameters: the stress difference s, which determines the friction line to be intersected, and δ, which defines the relative size of the inner circles. By using $\underline{\underline{T}}_d$ instead of $\underline{\underline{T}}$, we are replacing a figure where the friction line would be fixed and Mohr's circles varying in position and size with a fixed outer Mohr circle of diameter 1 and a friction line of varying position but constant slope; this makes superposition much easier. Using equation (53), the friction lines are labeled by their associated s value. The $\vec{s_1}$, $\vec{s_2}$, $\vec{s_3}$ solution trajectories correspond to the intersection of the friction line with the area between the outer and inner Mohr's circles.

Critical Cases

If s is smaller than s_c, the friction line does not intersect the outer Mohr's circle, and therefore slip cannot occur. This corresponds to searching a level curve of H_* with $V_0 > 1$ that does not exist (Table 4).

The smallest value of stress difference s for which the friction line intersect Mohr's circle is s_c (equation (38)). In other terms, for sliding to occur the stress difference must have reached the threshold s_c. For that value, $\vec{s_1}$, $\vec{s_2}$, $\vec{s_3}$, coincide with P_f, B, T_f (Figure 7) unless the tensor is degenerate (cases $\delta = 0$ or $\delta = 1$). P_f, B, T_f is then the most efficient orientation of the principal stresses, that is, that which produces slip at minimum stress level.

As s increases, the friction line slices deeper into Mohr's circles, and the nature of the trajectories of $\vec{s_1}$, $\vec{s_2}$, and $\vec{s_3}$ changes. Two critical cases that correspond to the tangence of the friction line with the two inner circles occur (Figure 7).

Also, if the friction line intersects the intermediate circle (that shown on Figure 3), that is, if the value of s is large enough so that V_0 is smaller than the absolute maximum of H_*^-, then the trajectory is made in part of an H_*^+ solution and in part of an H_*^- solution. However, this difference does not seem to have physical meaning, even though it has to be taken into

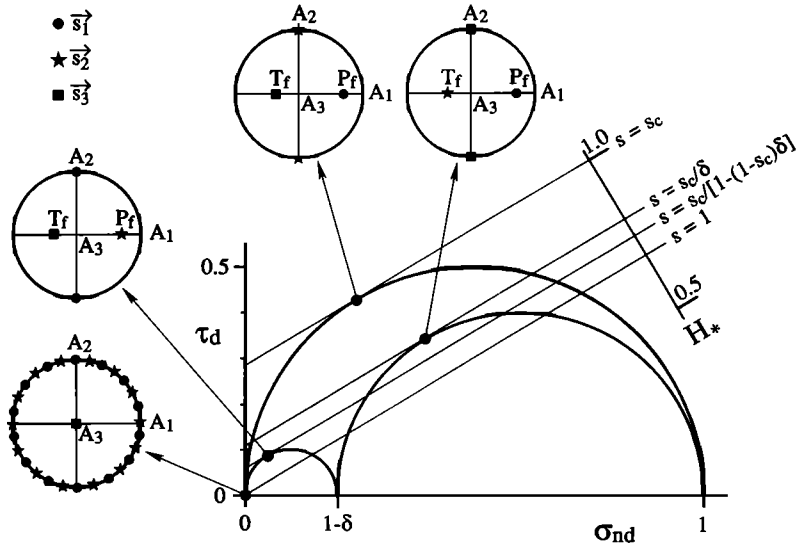

Fig. 7. Tangence of the friction lines $H_* = s_c / s$ with Mohr's circles. These tangences correspond to the three critical cases where the $\vec{s_1}$, $\vec{s_2}$, $\vec{s_3}$ orientations undergo significant physical changes. The orientations of the principal stresses corresponding to each case are shown in projection.

account in the substitution of ψ for correct results, and the following discussion is simplified by not distinguishing the $\varepsilon = +1$ ($\psi = \psi_1$) and $\varepsilon = -1$ ($\psi = \psi_2$) types of solutions.

Finally, because applying a friction law requires a compressive environment

$$0 \leq s < 1 \tag{54}$$

V_0 must satisfy

$$s_c < V_0 \tag{55}$$

This adds a fourth critical case: the lowest friction line that corresponds to $s = 1$ or $V_0 = s_c$ and passes through the origin.

We consider then only four critical cases, each of which corresponds to a relationship between s and δ. Figure 7 shows these limiting cases in Mohr's domain for the stress magnitudes and on Lambert's [1772] projection for the corresponding orientations of $\vec{s_1}$, $\vec{s_2}$, $\vec{s_3}$. The corresponding relationships divide the (δ, s) plane into five areas, four of which correspond to the four types of $\vec{s_1}$, $\vec{s_2}$, $\vec{s_3}$ trajectories (Figure 8). The evolutions between these types of trajectories can be easily understood if one concentrates on cross sections of the (δ, s) planes at either δ or s constant.

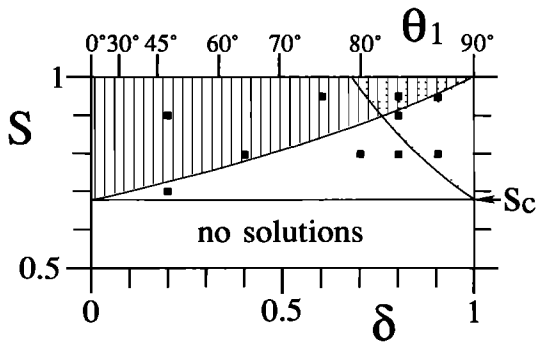

Fig. 8. Critical boundaries in the (δ, s) plane corresponding to the critical cases of Figure 7. To each curved polygon correspond a type of $\vec{s_1}$, $\vec{s_2}$, $\vec{s_3}$ trajectories; the lined and dotted areas correspond to tensors that satisfy the geometrical and frictional constraint and for which $\vec{s_1}$ and $\vec{s_3}$, respectively, can lie in the fault plane along the B axis, therefore totally exchange roles with $\vec{s_2}$. The white area where $s \geq s_c$ corresponds to those tensors for which neither $\vec{s_1}$ nor $\vec{s_3}$ can lie on the B axis once the constraints are satisfied. The white area where $s \leq s_c$ corresponds to tensors that cannot satisfy the frictional constraint because their stress difference is too small to cause sliding. The squares designate the trajectories that are displayed in Figures 9,10,12, and 13.

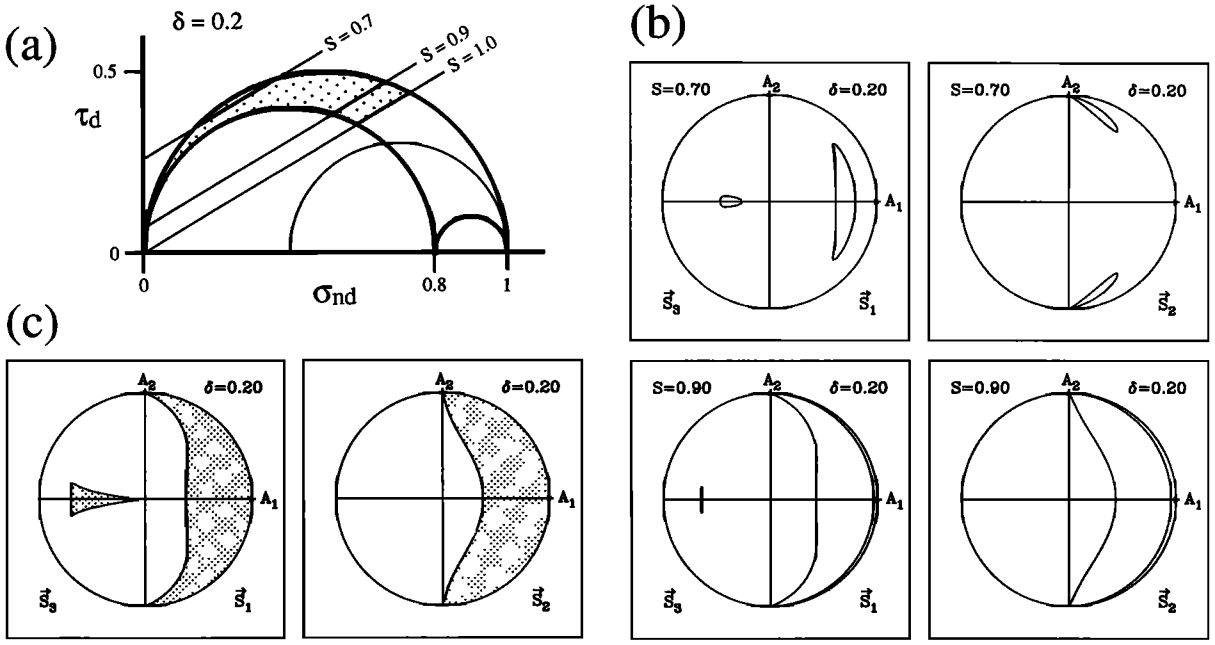

Fig. 9. Typical solution tensors with $\delta = 0.2$. (a) Mohr's circle. The dotted area, limited by the friction line $s = 1$, corresponds to all the acceptable solutions. There are only two typical cases: the friction line intersects either the outer circle only ($s = 0.7$) or both the outer and the left inner circle ($s = 0.9$). (b) Orientations of the principal stresses. (Left) $\vec{s_1}$ and $\vec{s_3}$ trajectories in the dilatational and compressional quadrant respectively. (Right) $\vec{s_2}$ trajectories. These trajectories correspond to the friction lines shown in Figure 9a. (c) Area spanned by the orientations of the principal stresses (dotted pattern); it corresponds to the dotted area in Figure 9a. Note that $\vec{s_1}$ does not fill up the whole R_G area.

Trajectories at δ Fixed

The representation at fixed δ has the advantage first, that Mohr's circles are fixed, therefore as s varies, only the friction line moves (Figures 7, 9a, and 10a), and second, that the $\vec{s_2}$ trajectories for different s do not cross each other (Figure 11). The drawback is that the $\vec{s_1}$ and $\vec{s_3}$ trajectories for different s do cross each other. As the friction line slices more and more deeply into Mohr's circles, the corresponding solution orientations of $\vec{s_1}$, $\vec{s_2}$, $\vec{s_3}$ are shown for two cases: δ = 0.2 (Figure 9) and δ = 0.8 (Figure 10).

For $s \leq s_c$ there cannot be any movement on the fault plane. For $s = s_c$, $\vec{s_1}$, $\vec{s_2}$, $\vec{s_3}$ coincide with P_f, B, T_f (Figure 7). As s increases above s_c, the friction line slices deeper into Mohr's circle and $\vec{s_1}$, $\vec{s_2}$, $\vec{s_3}$ start moving away from P_f, B, T_f, hence $\vec{s_2}$ starts to move away from the fault plane (Figures 9a and 9b with s = 0.7 and Figures 10a and 10b with s = 0.8). If s increases more, the friction line will start intersecting one of the two lower circles, and this will have different effects according to which circle is intersected.

If the circle of diameter $\sigma_2 - \sigma_3$ is intersected, then $\vec{s_1}$ reaches the fault plane in A_2 and $\vec{s_2}$ replaces $\vec{s_1}$ on A_1A_3, $\vec{s_3}$ keeping its position on A_1A_3 (Figures 9a and 9b with s = 0.9). This happens if and only if (Figures 7 and 8)

$$s \geq s_c / [1 - (1 - s_c)\,\delta] \tag{56}$$

When that circle is not intersected, the closer to it the friction line approaches, the more $\vec{s_1}$ and $\vec{s_2}$ tend to exchange roles.

If the circle of diameter $\sigma_1 - \sigma_2$ is intersected, then $\vec{s_3}$ reaches the fault plane and $\vec{s_2}$ and replaces $\vec{s_3}$ on the A_1A_3 plane, $\vec{s_1}$ keeping its position on A_1A_3 (Figures 10a and 10b with s = 0.9). This happens if and only if (Figures 7 and 8)

$$s \geq s_c / \delta \tag{57}$$

The closer to that circle the friction line approaches, the more $\vec{s_3}$ and $\vec{s_2}$ tend to exchange roles.

The order in which theses events occur as s increases depends only on the size ratio of the different inner circles, hence on δ.

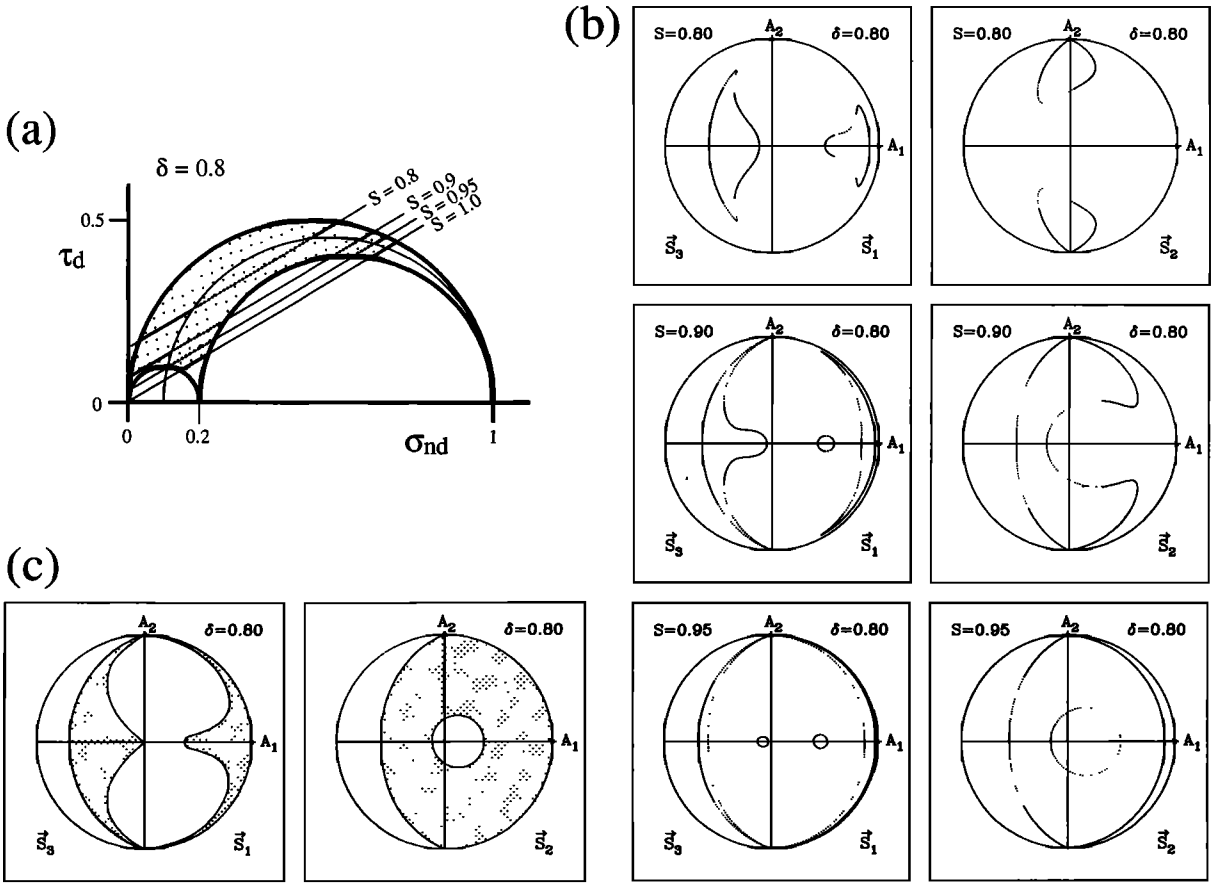

Fig. 10. Typical solution tensors with δ = 0.8. The dotted trajectories and friction lines correspond to ε = -1, the solid ones to ε = +1. Besides the two typical cases already shown for δ = 0.2 (Figure 9), a third one appears where the friction line intersects both inner circles (s = 0.95), and therefore $\vec{s_2}$ exchanges positions with both $\vec{s_1}$ or $\vec{s_3}$. As a result, the domain covered by $\vec{s_2}$ is greatly extended.

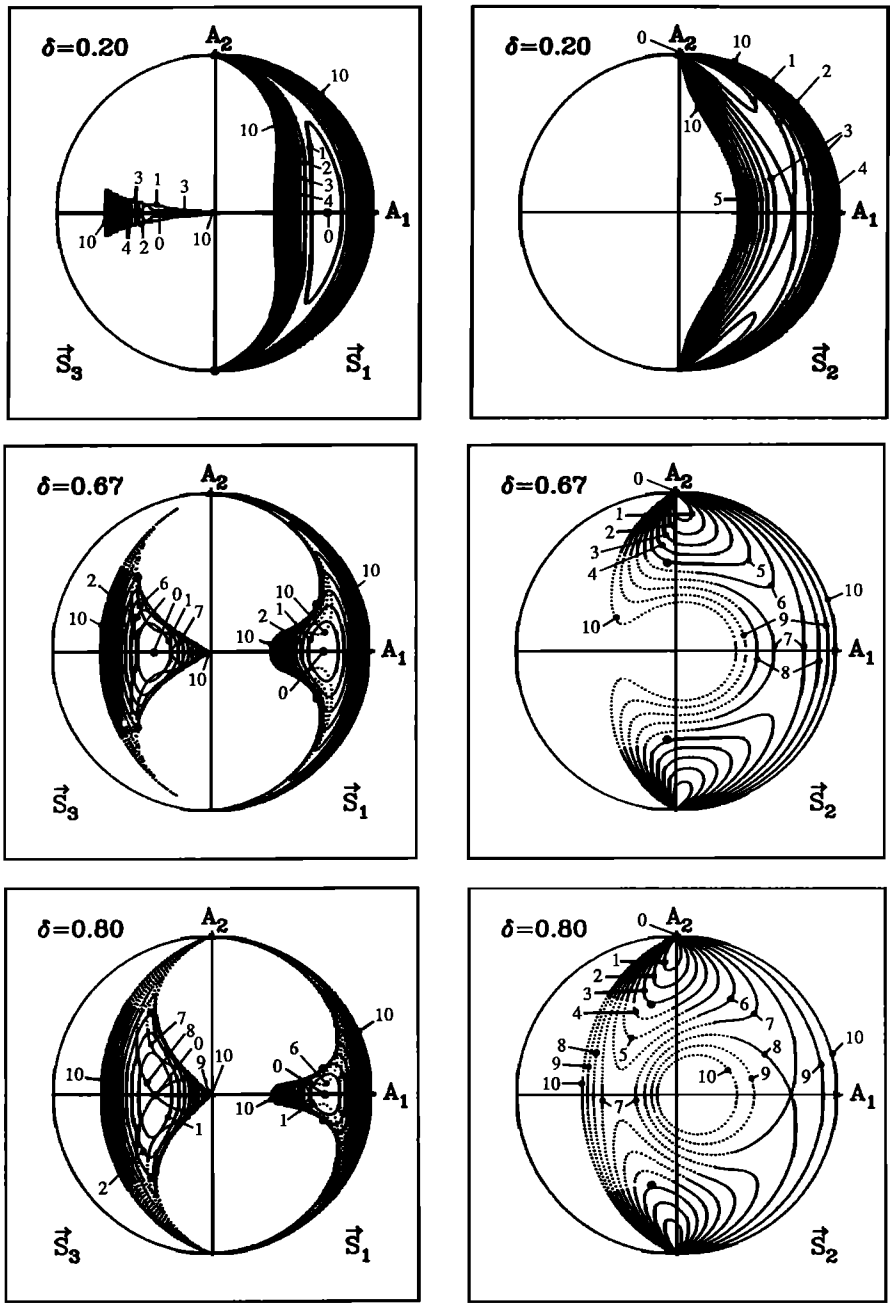

Fig. 11. The $\vec{s_1}$, $\vec{s_2}$, $\vec{s_3}$ trajectories for solution tensors at fixed δ. The trajectories from $s = s_c$ to $s = 1$ by increment of $(1-s_c)/10$ are labeled from 0 to 10 in that order. (Left) $\vec{s_1}$ and $\vec{s_3}$ trajectories. (Right) $\vec{s_2}$ trajectories. Solid curves, $\varepsilon = +1$; dotted curves, $\varepsilon = -1$.

In general, the higher the stress difference, the farther away from P_f, B, and T_f must $\vec{s_1}$, $\vec{s_2}$, and $\vec{s_3}$ be. In other words if the stress difference is high, $\vec{s_1}$, $\vec{s_2}$, $\vec{s_3}$ must have been poorly oriented for the movement not to occur earlier (at lower s), and according to which inner circle is bigger, $\vec{s_2}$ will tend to exchange roles with either $\vec{s_1}$ or $\vec{s_3}$. The highest value that s can reach in a compressive environment is 1, which corresponds to a friction line going through σ_3 on the σ_n axis (Figure 7).

The space spanned by $\vec{s_1}$ is included in the R_G domain because the the geometrical constraint is satisfied [McKenzie, 1969], but it does not fill it, especially around A_3 (Figures 9c

and 10c), because it is limited by the contours corresponding to

$$s = 1 \quad \text{or} \quad V_0 = s_c \tag{58}$$

$$s = s_c \quad \text{or} \quad V_0 = 1 \tag{59}$$

The R_G domain can be split into three areas (Figure 11): (1) an area where both solution $\varepsilon = +1$ and $\varepsilon = -1$ are allowed; for any location of $\vec{s_1}$ within that area, two orientations of $\vec{s_2}$, $\vec{s_3}$, corresponding to ψ_1 and ψ_2, are then allowed; (2) an area where only $\varepsilon = +1$ solutions are allowed and where to any location of $\vec{s_1}$ corresponds only one acceptable orientation of $\vec{s_2}$, $\vec{s_3}$ determined by ψ_1; and (3) an area where no solutions exist because the tensors that satisfy the geometrical constraint do not satisfy the frictional constraint; this area corresponds to the solutions that would be accepted by an inversion based on the sole geometrical constraint but that are mechanically unsound because they would yield too small a shear stress compared to the normal stress across the fault plane to produce any sliding.

Trajectories at s Fixed

This representation has qualities converse of those at constant δ: the drawback is that as δ varies, so do the Mohr's circles (Figures 12a and 13a) and that the $\vec{s_2}$ trajectories tend to

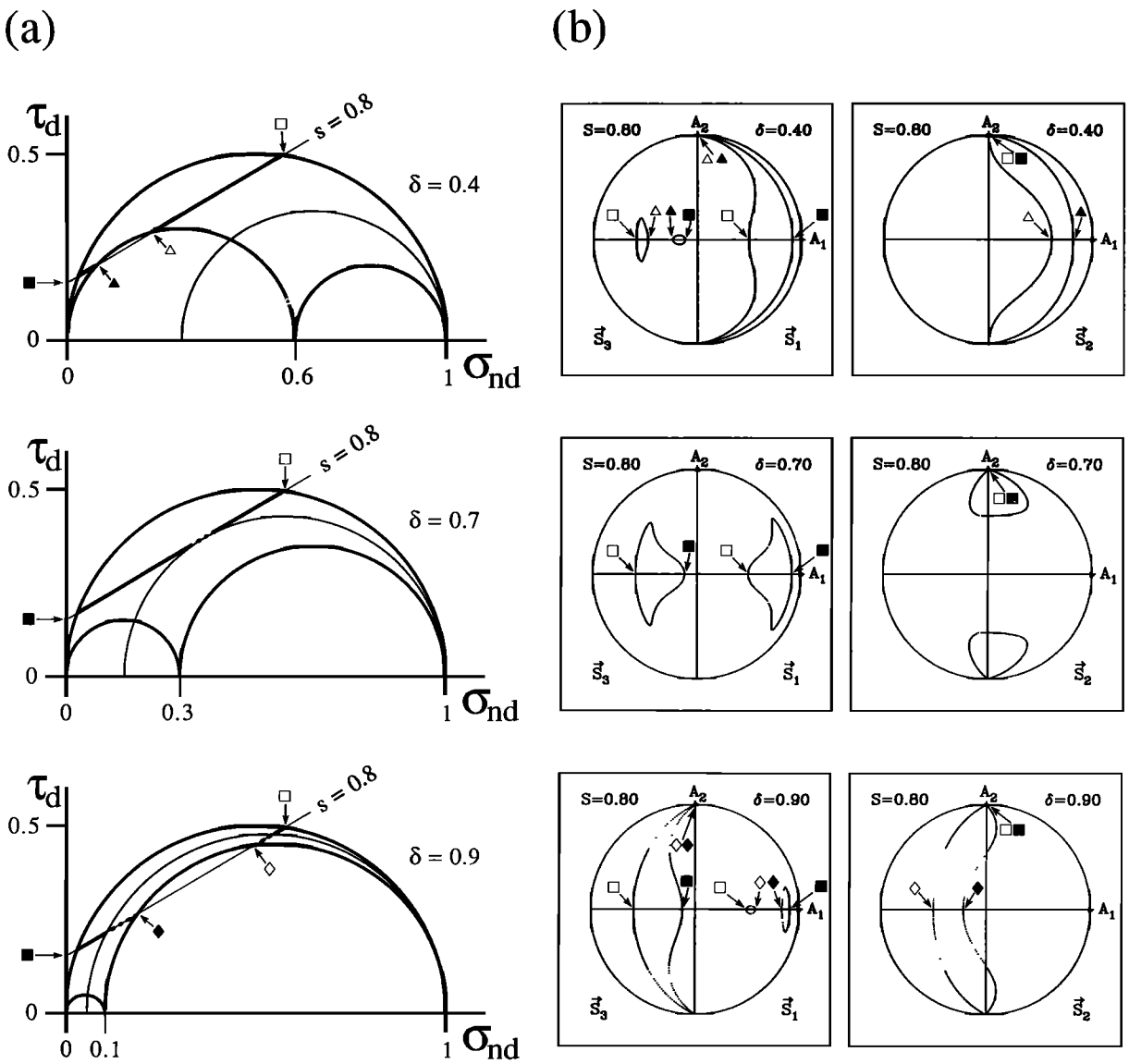

Fig. 12. Typical solution tensors with s = 0.8. (a) Mohr's circles (b) Trajectories of the principal stresses. The symbols correspond to those in Figure 12a.

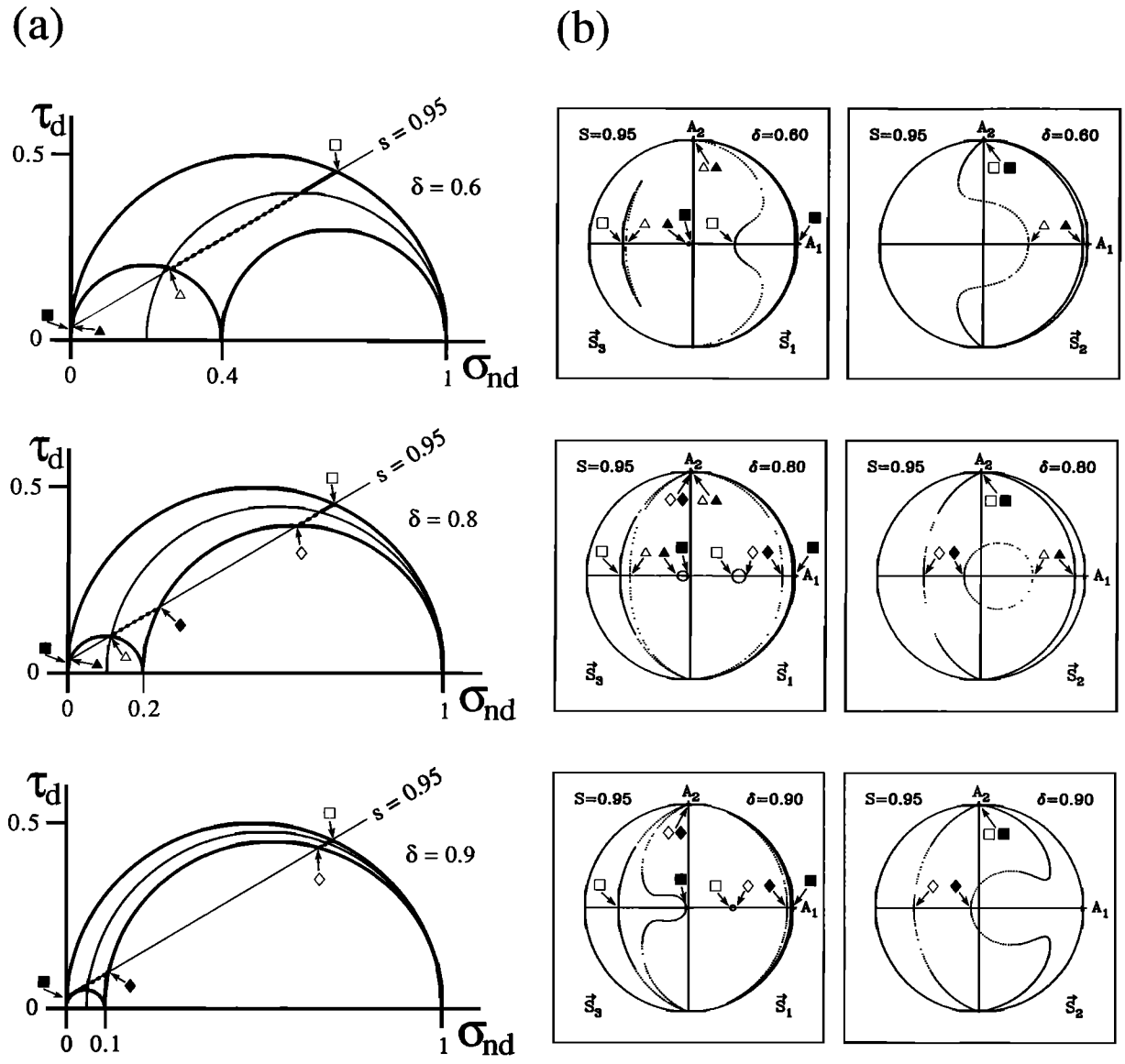

Fig. 13. Typical solution tensors with s = 0.95.

cross each other (Figure 14); the advantage is that the $\vec{s_1}$ and $\vec{s_3}$ trajectories for different δ do not cross each others.

If $s < s_c$, no slippage can occur. If $s = s_c$ (Figure 14 for s = 0.68), the least stress difference for which slippage can occur, three cases can be distinguished: (1) $\delta \neq 0$ and $\delta \neq 1$ (i.e., $\sigma_1 \neq \sigma_2$ and $\sigma_3 \neq \sigma_2$) and then $\vec{s_1}$ lies on the P_f axis (Figure 7), a position already recommended by Raleigh et al. [1972], while $\vec{s_2}$ and $\vec{s_3}$ are in B and T_f, respectively; (2) $\delta = 0$ (i.e., $\sigma_1 = \sigma_2$) and then $\vec{s_1}$ and $\vec{s_2}$ describe the great circle going through P_f and B, while $\vec{s_3}$ is in T_f; (3) $\delta = 1$ (i.e., $\sigma_3 = \sigma_2$) and then $\vec{s_2}$ and $\vec{s_3}$ describe the great circle going through T_f and B, while $\vec{s_1}$ is in P_f.

For $s_c < s \leq s_c (2 - s_c)$ (Figure 12 and 14 for any value $0.68 < s < 0.9$), two cases can be distinguished according to the values of δ: either (1) the inner Mohr's circles are not intersected and the orientations of the principal stresses $\vec{s_1}$, $\vec{s_2}$, $\vec{s_3}$ stay reasonably close to where they are classically expected, that is, close to P_f, B, T_f; or (2) one of the inner circles is intersected and $\vec{s_2}$ may interchange position with either $\vec{s_1}$ or $\vec{s_3}$. But because both inner circles cannot be intersected for any given value of δ, $\vec{s_2}$ can never exchange roles with both $\vec{s_1}$ and $\vec{s_3}$. Therefore if one of $\vec{s_1}$ or $\vec{s_3}$ tends to be delocalized and away from where classically expected, the other one will tend to be localized around its classical position.

For $s_c (2 - s_c) \leq s < 1$ (Figures 13 and 14 for any value $s \geq 0.9$), the same behavior is observed, but there is also a

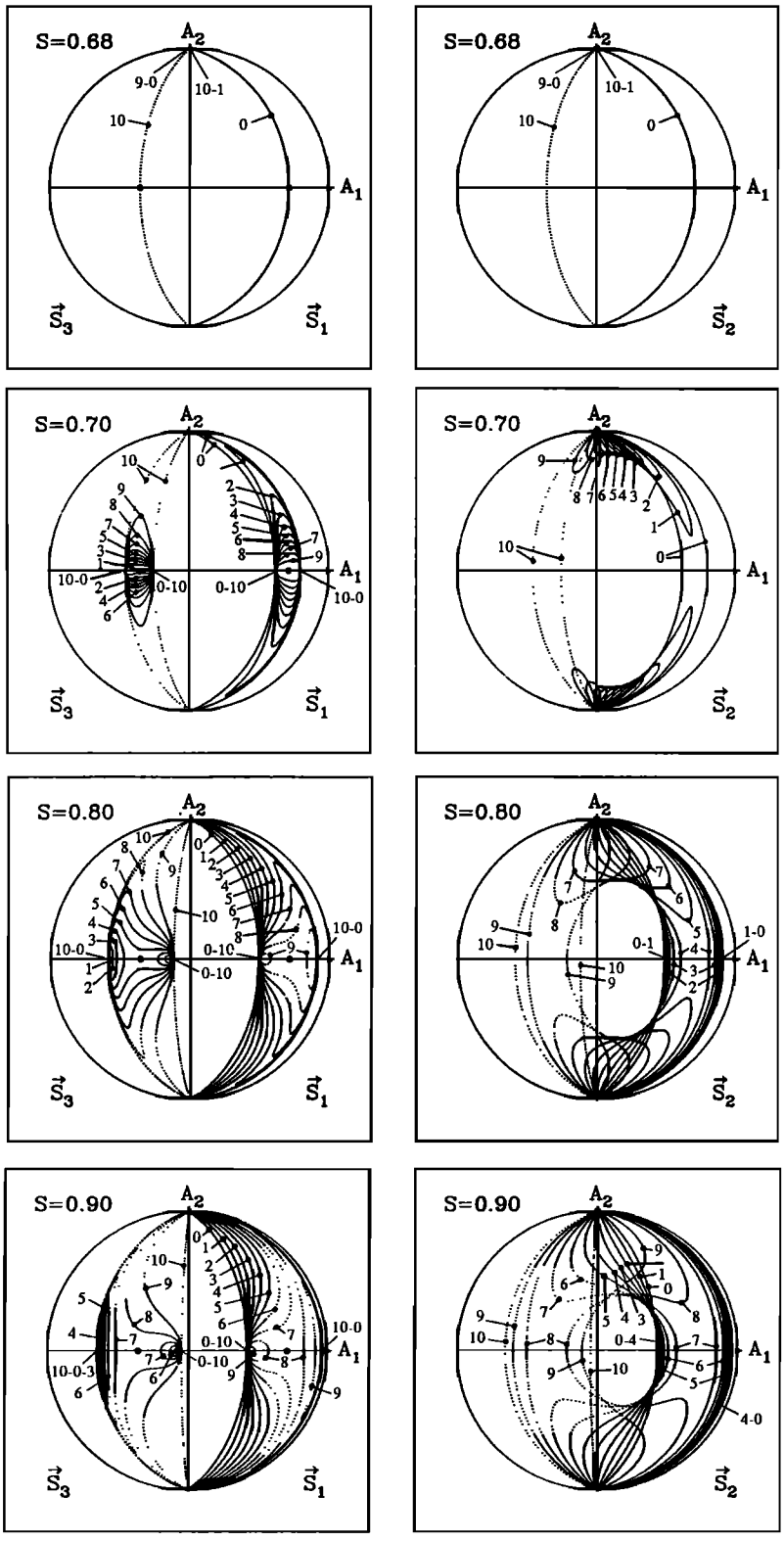

Fig. 14. The $\vec{s_1}$, $\vec{s_2}$, $\vec{s_3}$ trajectories for solution tensors at fixed s. The 11 trajectories for δ varying from 0 to 1 by increment of 1/10 are labeled from 0 to 10 in that order.

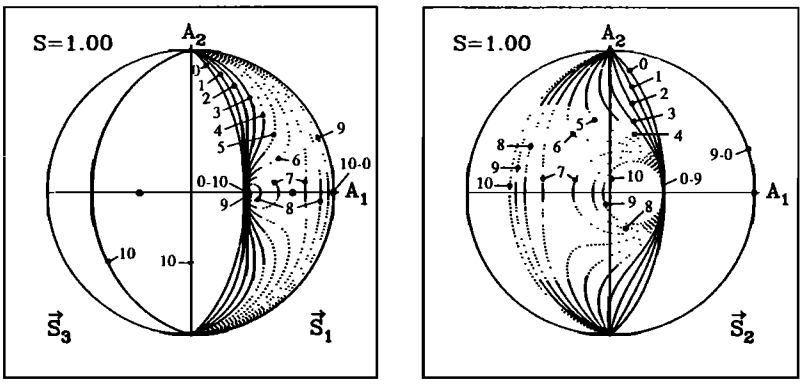

Fig. 14. (continued)

range of value of δ for which both inner circles are intersected and therefore $\vec{s_2}$ can exchange position with either $\vec{s_1}$ or $\vec{s_3}$; that is, slip can occur on both modes of unexpected stress orientations.

If s = 1, the area where $\vec{s_1}$ can be reaches its maximum extent (Figure 14); it is bounded by a great circle at angle φ_0 from the fault plane normal and by the fault plane itself. However, this is a limiting case because it corresponds to either $\sigma_1 = \infty$ or $\sigma_3 = 0$. The first case can be safely ruled out because of the finite strength of rocks. The second case may violate the condition of positive normal stress required by the friction law (equation (42)); since it applies to effective stress, it may correspond to a case where pore pressure is equal to the least principal stress magnitude and is appropriately described by hydrofracturing or tensional cracking as opposed to frictional sliding.

The domains spanned by $\vec{s_1}$, $\vec{s_2}$, $\vec{s_3}$ when s is fixed can be described as follow (Figure14): the set of $\vec{s_1}$ trajectories which correspond to various values of δ is bounded by two great circles that correspond to the degenerate case $\delta = 0$ ($\sigma_2 = \sigma_1$); the limits for $\vec{s_3}$ can be obtained in the same fashion by the case $\delta = 1$ ($\sigma_2 = \sigma_3$); the maximum area allowed to $\vec{s_2}$ is larger than the union of the area for $\vec{s_1}$ and $\vec{s_3}$ especially around A_2 (or B axis); its exact boundary is therefore not as simple.

The area spanned by $\vec{s_1}$, $\vec{s_2}$, $\vec{s_3}$ for any value of s includes the area spanned for any smaller value of s. This means the higher the stress difference, the worse oriented the principal stresses can afford to be in respect to the fault plane and still cause slippage. The maximum range is therefore obtained for s = 1.

The influence of σ_2 (or δ) [Bott, 1959; Jaeger and Rosengren, 1969] on the directions of the principal stresses is displayed by the δ dependence of the $\vec{s_1}$, $\vec{s_2}$, $\vec{s_3}$ trajectories at s fixed. As δ goes to 0 (σ_2 becomes close to σ_1), $\vec{s_1}$ and $\vec{s_2}$ tend to exchange roles, whereas as δ goes to 1 (σ_2 becomes close to σ_3), $\vec{s_3}$ and $\vec{s_2}$ tend to exchange roles. For $s = s_c$ the only cases where $\vec{s_2}$ can exchange roles with $\vec{s_3}$ or $\vec{s_1}$ are $\delta = 0$ and $\delta = 1$; as s increases above s_c, such cases occur for δ farther and farther away from 0 or 1 (Figure 8).

Therefore the orientations allowed for $\vec{s_1}$ and $\vec{s_3}$ can be globally described as controlled in width by s and in span by δ.

CONCLUSIONS

1. When both the geometrical and frictional constraints are required, there are still four degrees of freedom among the solution tensors $\underline{\underline{T}}$. One such degree, the scaling factor σ_1, can be removed and the resulting tensor $(1/\sigma_1) \bullet \underline{\underline{T}}$ depends on five parameters, θ, φ, ψ, δ, s, and exhibits three degrees of freedom. There is then a whole family of solution tensors, but for these tensors there is a relationship between the magnitudes, δ and s, and the orientations, θ, φ, ψ, of the principal stresses; a fixed orientation corresponds to a relationship between δ and s (equation (51)), and fixed relative magnitudes, δ and s, correspond to a trajectory for each of $\vec{s_1}$, $\vec{s_2}$ and $\vec{s_3}$.

2. If the lithosphere is isotropically fractured, as assumed by Brace and Kohlstedt [1980], there is always a plane of weakness along the most favorable orientation for frictional sliding, and when failure occurs, it occurs along that plane; it therefore behaves like a weak intact material [Talobre, 1957; Jaeger, 1962]. This is an isotropic problem; therefore s must be equal to s_c, the minimal stress difference that can cause sliding; $s_c = 0.679$ (equation (52)) corresponds exactly to $\sigma_1 \approx 3\sigma_3$ proposed by Brace and Kohlstedt [1980] because both results are based on Byerlee's [1978] friction coefficient (equation (44)). The vectors $\vec{s_1}$, $\vec{s_2}$, $\vec{s_3}$ must be on the P_f, B, and T_f axes with the exception of degenerate tensors where either half the circle $C(\varphi_1)$ would be allowed for $\vec{s_2}$ and $\vec{s_1}$ (case $\sigma_2 = \sigma_1$) or half the circle $C(\pi/2\text{-}\varphi_1)$ for $\vec{s_2}$ and $\vec{s_3}$ (case $\sigma_2 = \sigma_3$).

3. If the planes of weakness do not span all orientations, but any orientation is at a small angle to a plane of weakness, then the stress difference s is unlikely to reach too high values; then, unless the stress tensor is close to a degenerate case (i.e., unless σ_2 is close to σ_1 or σ_3), $\vec{s_1}$, $\vec{s_2}$, and $\vec{s_3}$ will remain reasonably close to P_f, B, and T_f. This explains why the classical P, B, T axes, which are only 15° away from these orientations, give reasonable answers [Scheidegger, 1964] despite objections [McKenzie, 1969]. However, if the fault

plane can be identified, P_f, B, and T_f give more accurate estimates, as already suggested by Raleigh et al. [1972] on the basis of a two-dimensional study.

4. In areas where a few major faults are known to be reactivated over and over again the former assumptions might not hold true, and s may be limited only by the strength of the rocks. As s increases, $\vec{s_1}$ and $\vec{s_3}$ may move away from P_f and T_f within the A_1A_3 plane. Furthermore, according to the value of δ, $\vec{s_1}$ and $\vec{s_3}$ may also go significantly away from that A_1A_3 plane toward the B axis in the fault plane, where $\vec{s_2}$ would be expected, while $\vec{s_2}$ may go out of the fault plane toward the A_1A_3 plane where $\vec{s_1}$ and $\vec{s_3}$ would be expected. There is then a tendency for $\vec{s_2}$ to exchange roles with either $\vec{s_1}$ or $\vec{s_3}$. The conditions on (δ,s) for such exchanges to be possible are summarized in Figure 8.

5. If the only available data are a single fault plane, then the stress tensor must verify $s \geq s_c$ and $\vec{s_1}$, $\vec{s_2}$ $\vec{s_3}$ may lie anywhere in the regions allowed for s = 1 (Figure 15a). These areas are significantly smaller than those obtained obtained by considering the geometrical constraint alone [McKenzie, 1969; Angelier and Mechler, 1977]. Moreover, fresh failure is expected to limit the stress difference so as $s \leq s_c' < 1$, where s_c' is determined by the failure properties for intact rocks as opposed to the frictional ones. Data for quartz rheologies [Ohnaka, 1973] suggest that fresh failure is likely to occur for s above the critical value $s_c' \approx 0.8$. As a result, the orientations

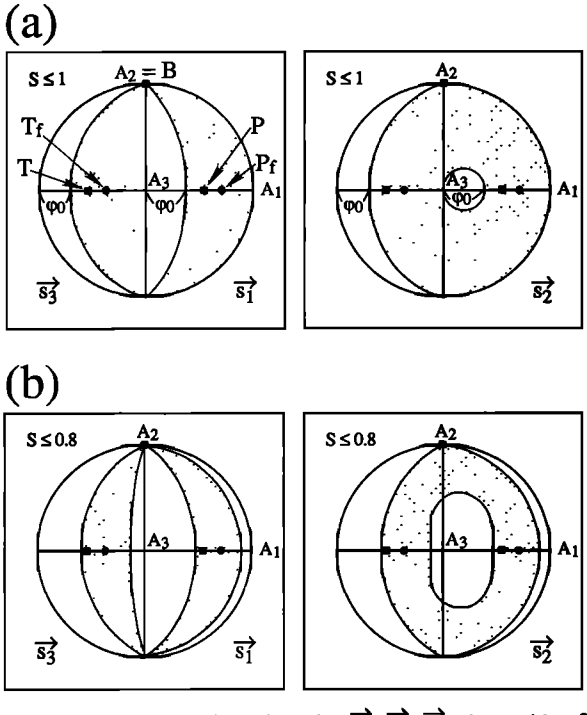

Fig. 15. Range of orientations for $\vec{s_1}$, $\vec{s_2}$, $\vec{s_3}$ when neither δ nor s are known and (a) one does not assume anything about s or (b) one assumes that s is limited by failure on intact plane to $s \leq s_c' = 0.8$.

of the principal stresses are limited to the more restricted domains obtained for s = 0.8 (Figure 15b). It may be useful to remember that the simple two-dimensional analysis for $\sigma_2 = \sigma_1$ and $\sigma_2 = \sigma_3$ gives the extreme bounds for the orientation of $\vec{s_1}$ and $\vec{s_3}$, respectively, as suggested by Wallace [1951]. Also, if by other means the orientation of $\vec{s_1}$ is determined, then s and δ are linked (equation (51)) and therefore an estimate of the stress difference s can be translated into an estimate of the aspect ratio δ.

6. If multiple fault planes are available and one assumes that the same stress tensor is responsible for the movement on all of them, two methods can be implemented: (1) a graphic method in which one intersects the areas allowed to $\vec{s_1}$, $\vec{s_2}$, and $\vec{s_3}$ for each fault plane and so localizes the orientations of the principal stresses; this is an improvement on the dihedra method [Angelier and Mechler, 1977] because the areas to intersect are smaller; then going back into each fault plane, the determined position of $\vec{s_1}$ yields an equation in (s, δ), and the resulting overdetermined system in (s, δ) can be examined; and (2) an inverse method in which it seems that the extra constraint brought by the friction law allows to invert for s on top of δ, $\vec{s_1}$, $\vec{s_2}$, and $\vec{s_3}$; unless the tensor is close to a degenerate one, at reasonable stress level $\vec{s_1}$ and $\vec{s_3}$ cannot have a wide range of variation; therefore, in that case, widely different plane orientations would require a higher stress difference than clustered ones; the fault plane orientations therefore contains information not only about δ but also about s, and this information could be extracted.

For both methods the extra frictional constraint reduces the chances of finding an acceptable uniform tensor solution, while it increases the chances of demonstrating the necessity of a spatially or temporally varying tensor.

Acknowledgments. This work was initiated by W. F. Brace's suggestion to add a frictional law to the geometrical constraint commonly used in this problem; his course provided also many sources of inspiration. I am grateful to K. Aki, P. Molnar, and J. G. Sclater for encouragements and comments; to M. McNutt and B. Parsons for free computer access; and to K. Craeger and D. Krowitz for help with the computer system. I am also indebted to D. Forsyth for a very helpful and thorough review.

REFERENCES

Amontons, G., De la résistance causée dans les machines, *Mem. Acad. R. Sci. Paris*, 206-222, 1699.

Anderson, E.M., *The dynamics of faulting and dyke formation with applications to Britain*, 2nd ed., 206 pp., Oliver and Boyd, Edinburgh, 1951.

Angelier, J., Sur l'analyse de mesures recueillies dans des sites faillés: l'utilité d'une confrontation entre les méthodes dynamiques et cinématiques, *C. R. Acad. Sci., Ser. D, 281*, 1805-1808, 1975.

Angelier, J., Determination of the mean principal directions of

stresses for a given fault population, *Tectonophysics, 56*, T17-T26, 1979a.

Angelier, J., Néotectonique de l'arc egéen, *Spec. Publ. Soc. Geol. Nord., 3*, 418 pp., 1979b.

Angelier, J., and J. Goguel, Sur une méthode simple de détermination des axes principaux des contraintes pour une population de failles, *C. R. Acad. Sci., Ser. D, 288*, 307-310, 1979.

Angelier, J., and P. Mechler, Sur une méthode graphique de recherche des contraintes principales également utilisable en tectonique et en sismologie: la méthode des dièdres droits, *Bull. Soc. Geol. Fr., XIX(6)*, 1309-1318, 1977.

Angelier, J., A. Tarantola, B. Valette, and S. Manoussis, Inversion of field data in fault tectonics to obtain the regional stress, I, Single phase fault populations: a new method of computing the stress populations, *Geophys. J. R. Astron. Soc., 69*, 607-621, 1982.

Armijo, R., and A. Cisternas, Un problème inverse en microtectonique cassante, *C. R. Acad. Sci., Ser. D, 287*, 595-598, 1978.

Armijo, R., E. Carey, and A. Cisternas, The inverse problem in microtectonics and the separation of tectonic phases, *Tectonophysics, 82*, 145-160, 1982.

Bott, M.H.P., The mechanics of oblique slip faulting, *Geol. Mag., 96*, 109-117, 1959.

Brace, W.F., and D.L. Kohlstedt, Limits on lithospheric stress imposed by laboratory experiments, *J. Geophys. Res., 85*, 6248-6252, 1980.

Byerlee, J.D., Frictional characteristics of granite under high confining pressure, *J. Geophys. Res., 72*, 3639-3648, 1967.

Byerlee, J.D., Friction of rocks, *Pure Appl. Geophys., 116*, 615-626, 1978.

Carey, E., Analyse numérique d'un modèle mécanique élémentaire appliqué à l'étude d'une population de failles: calcul d'un tenseur moyen des contraintes à partir des stries de glissement, thèse, 138 pp., Univ. de Paris Sud, 1976.

Carey, E., Recherche des directions principales de constraintes associées au jeu d'une population de failles, *Rev. Geol. Dyn. Geogr. Phys., 21*, 57-66, 1979.

Carey, E., and B. Brunier, Analyse théorique et numérique d'un modèle mécanique élémentaire appliqué à l'étude d'une population de failles, *C. R. Acad. Sci., Ser. D, 279*, 891-894, 1974.

Célérier, B., Constraint on stress tensor from slip on a single fault plane, *Tech. Rep. 73*, 95 pp., Inst. for Geophys., Univ. of Texas, Austin, 1987.

Coulomb, C.A., Sur une application des règles maximis et minimis à quelques problèmes de statique relatifs à l'architecture, *Acad. Sci. Paris Mém. Math. Phys., 7*, 343-382, 1776.

Donath, F.A., Strength variation and deformational behaviour in anisotropic rock, in *State of stress in the earth's crust*, edited by W.R. Rudd, pp. 280-298, American Elsevier, New York, 1964.

Ellsworth, W.L., A general theory for determining state of stress in the earth from fault slip measurements, *Terra Cognita, 2*, 170-171, 1982.

Ellsworth, W.L., and X. Zhonghuai, Determination of the stress tensor from focal mechanism data, *Eos Trans. AGU, 61*, 1117, 1980.

Etchecopar, A., G. Vasseur, and M. Daignieres, An inverse problem in microtectonics for the determination of stress tensors from fault striation analysis, *J. Struct. Geol., 3*, 51-65, 1981.

Euler, L., Du mouvement d'un corps solide quelconque lorsqu'il tourne autour d'un axe mobile, *Mém. Acad. Sci. Berlin*, [16](1760), 176-227, 1767.

Gephart, J.W., and D.W. Forsyth, An improved method for determining the regional stress tensor using earthquake focal mechanism data: application to the San Fernando earthquake sequence, *J. Geophys. Res., 89*, 9305-9320, 1984.

Handin, J., Strength and ductility, in *Handbook of physical constants*, edited by S.P. Clark, Mem. Geol. Soc. Am., vol. 97, 223-289, 1966.

Handin, J., On the Coulomb-Mohr failure criterion, *J. Geophys. Res., 74*, 5343-5348, 1969.

Honda, H., and A. Masatuka, On the mechanisms of the earthquakes and the stresses producing them in Japan and its vicinity, *Sci. Rep. Tohohu Univ., Ser. 5, 4*, 42-60, 1952.

Jaeger, J.C., The frictional properties of joints in rock, *Geofis. Pura Appl., 43*, 148-158, 1959.

Jaeger, J.C., Shear fracture of anisotropic rocks, *Geol. Mag., 97*, 65-72, 1960.

Jaeger, J.C., *Elasticity, fracture and flow*, 2nd ed., 268 pp., Methuen, London, 1962.

Jaeger, J.C., Friction of rocks and stability of rock slopes, *Geotechnique, 21*, 97-134, 1971.

Jaeger, J.C., and N.C. Cook, *Fundamentals of rock mechanics*, 3rd ed., 593 pp., Chapman and Hall, London, 1979.

Jaeger, J.C., and K.J. Rosengren, Friction and sliding of joints, *Proc. Aust. Inst. Min. Metall., 229*, 93-104, 1969.

Lambert, J.H., *Beiträge zum Gebrauche der Mathematik und deren Anwendung, part III*, section 6, Anmerkungen und Zusätze zur Entwerfung der Land- und Himmelscharten, pp. 105-199, Berlin, 1772.

McKenzie, D.P., The relation between fault plane solutions for earthquakes and the directions of the principal stresses, *Bull. Seismol. Soc. Am., 59*, 591-601, 1969.

Michael, A.J., The determination of stress from slip data, faults and folds, *J. Geophys. Res., 89*, 11,517-11,526, 1984.

Mohr, O., Über die Darstellung des Spannungzustandes eines Korperelementes, *Civilingenieure, 28*, 113-156, 1882.

Mohr, O., Welche Umstände bedingen die Elastizitätsgrenze und den Bruch eines Materials, *Z. Ver. Dtsch. Ing., 44*, 1524-1530, 1572-1577, 1900.

Ohnaka, M., The quantitative effect of hydrostatic confining pressure on the compressive strength of crystalline rocks, *J. Phys. Earth, 21*, 125-140, 1973.

Palmer, F., What about friction?, *Am. J. Phys., 17*, 181-187, 327-342, 1949.

Rabinowicz, E., Resource Letter F-1 on friction, *Am. J. Phys., 31*, 897-900, 1963.

Raleigh, C.B, J.H. Healy, and J.D. Bredehoeft, Faulting and crustal stress at Rangely, Colorado, in *Flow and fracture of rocks*, edited by H.C. Heard, I.Y. Borg, N.L. Carter, and C.B. Raleigh, pp. 275-284, Geophys. Monogr. Ser., vol. 16, AGU, Washington, D.C., 1972.

Sassi, W., Analyse numérique de la déformation cassante, thèse de 3ème cycle, 229 pp., Univ. de Paris Sud à Orsay, 1985.

Scheidegger, A.E., The tectonic stress and tectonic motion direction in Europe and Western Asia as calculated from

earthquake fault plane solutions, *Bull. Seismol. Soc. Am., 54*, 1519-1528, 1964.

Talobre, J.A., *La mécanique des roches appliquée aux travaux publics*, 444 pp., Dunod, Paris, 1957.

Tresca, Mémoires sur l'écoulement des corps solides, *Mémoires présentés par divers savants*, Acad. Sci., Paris, vol. 18, 733-799, 1868.

Vasseur, G., A. Etchecopar, and H. Philip, Stress state inferred from multiple focal mechanisms, *Ann. Geophys., 1*, 291-298, 1983.

Wallace, R.E., Geometry of shearing stress and relation to faulting, *J. Geol., 59*, 118-130, 1951.

Zoback, M.D., and J.H. Healy, Friction, faulting, and in situ stress, *Ann. Geophys., 2*, 689-698, 1984.

B. Célérier, University of Texas, Institute for Geophysics, 8701 Mopac Boulevard, Austin, TX 78759-8345.

(Received July 11, 1986;
revised December 15, 1987;
accepted January 10, 1988.)